Improved α^4 term of the muon anomalous magnetic moment

Toichiro Kinoshita[1,*]

[1]*Laboratory for Elementary Particle Physics, Cornell University, Ithaca, New York, 14853 USA*

Makiko Nio[2,†]

[2]*Theoretical Physics Laboratory, RIKEN, Wako, Saitama, Japan 351-0198*

We have completed the evaluation of all mass-dependent α^4 QED contributions to the muon $g - 2$, or a_μ, in two or more different formulations. Their numerical values have been greatly improved by an extensive computer calculation. The new value of the dominant α^4 term $A_2^{(8)}(m_\mu/m_e)$ is 132.6823 (72), which supersedes the old value 127.50 (41). The new value of the three-mass term $A_3^{(8)}(m_\mu/m_e, m_\mu/m_\tau)$ is 0.0376 (1). The term $A_2^{(8)}(m_\mu/m_\tau)$ is crudely estimated to be about 0.005 and may be ignored for now. The total QED contribution to a_μ is $116\,584\,719.58(0.02)(1.15)(0.85) \times 10^{-11}$, where 0.02 and 1.15 are uncertainties in the α^4 and α^5 terms and 0.85 is from the uncertainty in α measured by atom interferometry. This raises the standard model prediction by 13.9×10^{-11}, or about 1/5 of the measurement uncertainty of a_μ. It is within the noise of current uncertainty ($\sim 100 \times 10^{-11}$) in the estimated hadronic contributions to a_μ.

I. INTRODUCTION AND SUMMARY

The latest measured value of the anomalous magnetic moment of negative muon is [1]

$$a_{\mu^-}(\text{exp}) = 11\,659\,214(8)(3) \times 10^{-10} \quad (0.7\ \text{ppm}), \quad (1)$$

where $a_\mu \equiv \frac{1}{2}(g_\mu - 2)$ and the numerals eight and three in parentheses represent the statistical and systematic uncertainties in the last digits of the measured value. 1 ppm $= 10^{-6}$. The world average value $a_\mu(\text{exp})$ obtained from this and earlier measurements [2–5] is

$$a_\mu(\text{exp}) = 11\,659\,208(6) \times 10^{-10} \quad (0.5\ \text{ppm}). \quad (2)$$

This result provides the most stringent test of the standard model.

Unfortunately, such a test must wait for further improvement in the uncertainty of the hadronic corrections to a_μ [6–16]. The lowest-order hadronic vacuum-polarization effect has thus far been determined from two sources, (i) $e^+ e^-$ annihilation cross section, and (ii) hadronic τ decays. Several recent evaluations are listed in Table I. Their differences (except for the one obtained from the τ decay data) are due to different interpretations and treatments of basically identical data. However, they all agree that the measurement of the $e^+ e^-$ annihilation cross section, in particular, in the region below $\rho - \omega$ resonances, must be improved substantially in order to reduce the experimental uncertainty significantly. Such efforts are underway at several laboratories. Particularly interesting and promising is new radiative-return measurements [17]. On the other hand, it is not clear at present whether the value from the

τ-decay data can be improved much further because of the difficulty in evaluating more precisely the effect of isospin breaking [6,7].

A new theoretical development is an attempt to calculate the hadronic vacuum-polarization effect on muon $g - 2$ in lattice QCD [18].

The NLO hadronic contribution has been evaluated by two groups [8,19]:

$$\begin{aligned} a_\mu(\text{had.NLO}) &= -10.1(0.6) \times 10^{-10}, \\ a_\mu(\text{had.NLO}) &= -9.8(0.1)_{\text{exp}}(0.0)_{\text{rad}} \times 10^{-10}. \end{aligned} \quad (3)$$

The contribution from radiative corrections is identical in two papers. The small difference comes from the diagram in which two hadronic vacuum-polarizations are inserted in the second-order vertex diagram.

The contribution of hadronic light-by-light scattering to a_μ is more difficult to obtain a reliable value because it cannot utilize any experimental information and must rely solely on theory. After correction of a sign error, it seemed to have settled down to around [10–15]

TABLE I. Recent evaluations of lowest-order hadronic vacuum-polarization contribution to the muon $g - 2$. Some errors are separated according to their sources: measurement errors and radiative corrections. [9] mentions a procedural error separately.

Process	$a_\mu(\text{had.LO}) \times 10^{10}$	Reference
$e^+ e^-$ annihilation	$696.3(6.2)_{\text{exp}}(3.6)_{\text{rad}}$	[6]
$e^+ e^-$ annihilation	$694.8(8.6)$	[7]
$e^+ e^-$ annihilation	$692.4(5.9)_{\text{exp}}(2.4)_{\text{rad}}$	[8]
$e^+ e^-$ annihilation	$699.6(8.5)_{\text{exp}}(1.9)_{\text{rad}}(2.0)_{\text{proc}}$	[9]
τ decay	$711.0(5.0)_{\text{exp}}(0.8)_{\text{rad}}(2.8)_{\text{SU(2)}}$	[6]

*Electronic address: tk@hepth.cornell.edu
†Electronic address: nio@riken.jp

$$a_\mu(\text{had.1}-1) \sim 80(40) \times 10^{-11}. \qquad (4)$$

More recently, however, a considerably different value was reported [16]:

$$a_\mu(\text{had.1}-1) \sim 136(25) \times 10^{-11}, \qquad (5)$$

which moves the prediction of the standard model closer to the experiment. This was obtained by imposing the short-distance QCD constraints on the $\pi^0\gamma^*\gamma$ amplitude, which was overlooked in previous analyses. Further confirmation of this result by a first principle calculation in lattice QCD would be highly desirable.

The weak interaction effect is known to two-loop order. The latest values are [20,21]

$$a_\mu(\text{weak}) = 152(1) \times 10^{-11},$$
$$a_\mu(\text{weak}) = 154(1)(2) \times 10^{-11}, \qquad (6)$$

where (1) and (2) in the second line are the remaining theoretical uncertainty and Higgs mass uncertainty, respectively. Although the numerical difference between these values is insignificant for comparison with experiment, their approach to the fermionic triangle diagram seems to be different. We hope it is resolved before long.

The QED contribution $a_\mu(\text{QED})$, even though it is the predominant term of a_μ, has received little attention thus far because of its small error bars. The theoretical uncertainty comes predominantly from the α^4 term whose contribution to a_μ is about 3.3 ppm. The best value of $a_\mu(\text{QED})$ reported previously (Eq. (11) of [22]) was

$$a_\mu(\text{QED})_{\text{old}} = 116\,584\,705.7(1.25)(1.15)(0.5) \times 10^{-11}$$
$$= 116\,584\,705.7(1.8) \times 10^{-11}, \qquad (7)$$

where 1.25 and 1.15 come from the uncertainties in the calculated α^4 and estimated α^5 terms, respectively, and 0.5 is from the uncertainty in the fine structure constant α given in Eq. (17) of [22] obtained from the measurement and theory of a_e.

While updating $a_\mu(\text{QED})$, however, we discovered that the previous evaluation of the α^4 term suffered from an error in a group of 18 Feynman diagrams [23]. This affects both Eq. (11) and Eq. (17) of Ref. [22] so that (7) had to be revised. This discovery prompted us to reexamine all other α^4 terms contributing to $a_\mu(\text{QED})$.

The purpose of this paper is to report the result of this reexamination. We give a full account of

(1) new evaluation of mass-dependent α^4 term of a_μ in an alternate formulation,
(2) vastly improved numerical precision by an extensive numerical evaluation of 469 eighth-order Feynman diagrams, and
(3) new evaluation of the α^4 term that depends on three masses m_e, m_μ, m_τ $(0.1094(3) \times 10^{-11})$, which replaces the old value (0.23×10^{-11}) quoted in [24].

If one uses the latest value of α obtained from the atom interferometry measurement [25]:

$$\alpha^{-1}(a.i.) = 137.036\,000\,3(10) \quad [7.4 \text{ ppb}], \qquad (8)$$

the new estimate of the QED contribution becomes

$$a_\mu(\text{QED}) = 116\,584\,719.58(0.02)(1.15)(0.85) \times 10^{-11}, \qquad (9)$$

where 0.02 replaces the previous uncertainty 1.25 of the α^4 term in (7), an improvement of factor 60. The error 0.85 comes from the uncertainty in the fine structure constant $\alpha(a.i.)$ given in (8). Note that this error is larger than the corresponding error in (7) because we used $\alpha(a.i.)$ of (8) instead of the incorrect $\alpha(a_e)$ used in (7). The new value (9) is larger than (7) by 13.9×10^{-11}. A report on the improvement of a_e and $\alpha(a_e)$ is being prepared [26].

As is seen from (9), the largest source of QED error is now the α^5 term, which was previously estimated to be $6.29(1.15) \times 10^{-11}$ [24,27]. Although this is accurate enough for comparison with the current experimental data, a more precise value will become necessary in the future. It is being improved at present and will be reported shortly [28].

Let us now present an outline of our approach to $a_\mu(\text{QED})$ and a summary of results before going into details. The contribution of QED diagrams to a_μ can be written in the general form

$$a_\mu(\text{QED}) = A_1 + A_2(m_\mu/m_e) + A_2(m_\mu/m_\tau)$$
$$+ A_3(m_\mu/m_e, m_\mu/m_\tau), \qquad (10)$$

where $m_e, m_\mu,$ and m_τ are the masses of the electron, muon, and tau, respectively. Throughout this article we shall use the values $m_e = 0.510\,998\,902(21)$ MeV/c^2, $m_\mu = 105.6\,583\,568(52)$ MeV/c^2, and $m_\tau = 1777.05(29)$ MeV/c^2, respectively [29].

The renormalizability of QED guarantees that A_1, A_2, and A_3 can be expanded in power series in α/π with finite calculable coefficients:

$$A_i = A_i^{(2)}\left(\frac{\alpha}{\pi}\right) + A_i^{(4)}\left(\frac{\alpha}{\pi}\right)^2 + A_i^{(6)}\left(\frac{\alpha}{\pi}\right)^3 + ..., i = 1, 2, 3. \quad (11)$$

$A_1^{(n)}$ is known up to $n = 4$ from the study of the electron anomaly a_e [22,26]. $A_1^{(2)}$, $A_1^{(4)}$, and $A_1^{(6)}$ have been evaluated precisely by both numerical and analytic means. $A_1^{(8)}$ is currently being improved by an extensive computer work [26]. For the purpose of evaluating $a_\mu(\text{QED})$, however, we may use A_1 obtained from the measured value of the electron anomaly a_e [30] subtracting small contributions due to muon, hadron, and weak interactions [31].

It is easy to see that $A_2^{(2)} = A_3^{(2)} = A_3^{(4)} = 0$: they have no corresponding Feynman diagram. $A_2^{(4)}(m_\mu/m_e)$, $A_2^{(6)}(m_\mu/m_e)$, and $A_3^{(6)}(m_\mu/m_e, m_\mu/m_\tau)$ have been eval-

uated by numerical integration, asymptotic expansion in m_μ/m_e, power series expansion in m_e/m_μ, and/or analytic integration. They are [32–35]

$$A_2^{(4)}(m_\mu/m_e) = 1.094\,258\,282\,8(98),$$

$$A_2^{(4)}(m_\mu/m_\tau) = 7.8059(25) \times 10^{-5},$$

$$A_2^{(6)}(m_\mu/m_e) = 22.868\,379\,36(23), \quad (12)$$

$$A_2^{(6)}(m_\mu/m_\tau) = 36.054(21) \times 10^{-5},$$

$$A_3^{(6)}(m_\mu/m_e, m_\mu/m_\tau) = 52.763(17) \times 10^{-5},$$

where the errors are due to measurement uncertainty of m_μ and m_τ only. The most striking feature of the α^3 term is the large size of $A_2^{(6)}(m_\mu/m_e)$. It comes predominantly from diagrams involving a light-by-light scattering subdiagram, as was first discovered in [36] and improved by numerical calculation [24]. Since $A_2^{(6)}(m_\mu/m_e)$ is now known analytically [34], its uncertainty depends only on the uncertainty in the measurement of m_e/m_μ and is totally negligible.

The term $A_2^{(8)}(m_\mu/m_e)$ has been known by numerical integration only. A crude evaluation of contributing integrals made more than ten years ago [24], which was no more than an order of magnitude estimate, showed that $A_2^{(8)}(m_\mu/m_e)$ contributes only about 3 ppm to a_μ. Thus it seemed that it was good enough for comparison with the experiment. Now that a program error was found in a part of evaluation of $A_2^{(8)}(m_\mu/m_e)$ [23] and since the measurement of a_μ is becoming more precise, however, it is important to reexamine these calculations and eliminate algebraic error, if any, completely and reduce the computational uncertainty as much as possible.

Within the Feynman gauge two approaches had been developed for numerical integration of Feynman diagrams contributing to the anomalous magnetic moment [37]. An obvious and straightforward one is to evaluate each vertex individually and add them up. (This approach will be called *Version B* following [23].) Another one starts by combining several vertices into one with the help of the Ward-Takahashi identity

$$q_\mu \Lambda^\mu(p, q) = -\Sigma\left(p + \frac{q}{2}\right) + \Sigma\left(p - \frac{q}{2}\right), \quad (13)$$

where $\Lambda^\mu(p, q)$ is the sum of vertices obtained by inserting the external magnetic field in fermion lines of a self-energy diagram $\Sigma(p)$. $p \pm q/2$ is outgoing (incoming) muon momentum. Differentiating both sides of (13) with respect to q_ν one obtains

$$\Lambda^\nu(p, q) \simeq -q^\mu\left[\frac{\partial \Lambda_\mu(p, q)}{\partial q_\nu}\right]_{q=0} - \frac{\partial \Sigma(p)}{\partial p_\nu}. \quad (14)$$

Obviously one may start from either the left-hand side

(LHS) or right-hand side (RHS) of this equation to evaluate the anomalous magnetic moment. The approach based on the RHS and LHS will be called *Version A* and *Version B*, respectively. The former required some additional algebraic work but produced fewer integrals and ensured significant economy of computing time.

Evaluation of the α^3 term was carried out in both *Version A* and *Version B* [37]. But, for the α^4 term, in particular, for 126 diagrams containing a light-by-light scattering subdiagram, the *Version B* codes were so large that we chose initially to work only with *Version A*. For the reason discussed already we have now reevaluated them also in *Version B* [23]. We have now extended this effort to the remaining 108 diagrams and obtained their codes in *Version B*. Numerical evaluation shows that they are in good agreement with those of *Version A*. As a consequence *all* α^4 diagrams contributing to $A_2^{(8)}(m_\mu/m_e)$ have been confirmed by two or more independent formulations. We are confident that all codes are now free from any algebraic error.

The remaining problem concerns the reliability of numerical integration. As a matter of fact, values of some integrals were called into question shortly after the old result was published [38]. It turned out that this was caused mainly by the relatively poor statistical sampling of the integrand resulting from shortage of computing power then available [39]. The problem was made worse by the presence of severe nonstatistical errors that originate from round-off errors inherent in *all* computer calculation. This will be called *digit-deficiency errors*. Various techniques had to be introduced to alleviate this problem [40]. See Appendix B for details.

Now that the validity of codes is established we are justified to evaluate all integrals contributing to the α^4 term in either *Version A* or *Version B*, using vastly increased number of sampling points, made possible by the new generations of computers, and, at the same time, reducing *digit-deficiency* errors to a manageable level by various means. (See Appendix B.)

All integrals have been evaluated with successively increasing statistics over the period of more than ten years. Some preliminary results were reported from time to time [41]. Only the latest and most accurate results are listed in Tables II, III, IV, V, VI, VII, VIII, IX, X, XI, and XII. Although earlier results are not shown explicitly, they have played crucial roles in checking the reliability of numerical integration at every stages of calculation.

The majority of integrals in the *Version A* calculation were found to be consistent with the results in *Version B*. But some of them were found to differ considerably because of poor statistical samplings and the digit-deficiency (*d-d*) problem. Thus some *Version A* integrals have been reevaluated to reduce the *d-d* problem. Evaluations of both versions are combined in quadrature, whenever appropriate, to improve the statistics.

The latest value of $A_2^{(8)}(m_\mu/m_e)$ is

$$A_2^{(8)}(m_\mu/m_e) = 132.6823(72), \qquad (15)$$

which is larger by 5.2 than the old value [22]

$$A_2^{(8)}(m_\mu/m_e) = 127.50(41). \qquad (16)$$

The difference between (15) and (16) is partly accounted for by the correction of program error described in [23] but is mostly due to the fact that (16) suffered from poor statistics and the *digit-deficiency* problem.

There is also a small contribution to a_μ from the three-mass term $A_3^{(8)}(m_\mu/m_e, m_\mu/m_\tau)$ which arises from 102 diagrams containing two or three closed loops of vacuum-polarization (v-p) and/or light-by-light scattering (l-l) type. Results of numerical evaluation are given in (61)–(63). From these results we obtain

$$A_3^{(8)}(m_\mu/m_e, m_\mu/m_\tau) = 0.037\,594(83). \qquad (17)$$

This is smaller than the value 0.079 (3) quoted in [24], which corresponds to (62) obtained only from the diagrams containing l-l loop, which were thought to be dominant. The new result (17) shows that this assumption was not fully justified. Another term of order α^4 is $A_2^{(8)}(m_\mu/m_\tau)$ which is calculable from 469 Feynman diagrams. However, its contribution to a_μ is of order $(m_\mu/m_\tau)^2 \ln(m_\tau/m_\mu) A_2^{(8)}(1) \sim 0.005$ so that it may be safely ignored for now.

Collecting all results of orders α^4 and α^5 [27] we find $a_\mu(\mathrm{QED})$ given in (9). In conclusion we have found that the improvement of the α^4 term does not significantly affect the comparison of theory and experiment of a_μ. The net effect of our calculation is to enhance the QED prediction (7) by 13.9×10^{-11} and eliminate an important source of theoretical uncertainty. As far as QED is concerned, the α^5 term is now the most important source of uncertainty in a_μ. This is being improved [28]. The overall theoretical uncertainty of the standard model remains dominated by that of the hadronic vacuum-polarization effect.

II. CLASSIFICATION OF DIAGRAMS CONTRIBUTING TO $A_2^{(8)}(m_\mu/m_e)$

There are altogether 469 Feynman diagrams contributing to $A_2^{(8)}(m_\mu/m_e)$. Feynman integrals for these eighth-order vertex diagrams consist of 12 propagators integrated over four four-dimensional loop momenta. These diagrams have subdiagrams of (v-p) type and/or (l-l) type. The v-p subdiagrams found in $A_2^{(8)}(m_\mu/m_e)$ are as follows:

Π_2, which consists of one closed lepton loop of second-order.

Π_4, which consists of three proper closed lepton loops of fourth-order.

$\Pi_{4(2)}$, which consists of three lepton loops of type Π_4 whose internal photon line has a Π_2 insertion.

Π_6, which consists of 15 proper closed lepton loops of sixth-order.

The l-l diagrams we need are:

Λ_4, which consists of six proper closed lepton loops of fourth-order, with four photon lines attached to them.

$\Lambda_4^{(2)}$, which consists of 60 diagrams in which lepton lines and vertices of Λ_4 are modified by second-order radiative corrections.

We are now ready to classify the diagrams into four (gauge-invariant) groups:

Group I. Second-order muon vertex diagrams containing lepton v-p loops Π_2, Π_4, $\Pi_{4(2)}$ and/or Π_6. This group consists of 49 diagrams.

Group II. Fourth-order proper vertex diagrams containing lepton v-p loops Π_2 and/or Π_4. This group consists of 90 diagrams.

Group III. Sixth-order proper vertex diagrams containing a v-p loop Π_2. This group consists of 150 diagrams.

Group IV. Muon vertex diagrams containing an l-l subdiagram Λ_4 with additional 2nd-order radiative corrections, or one of $\Lambda_4^{(2)}$ type. This group consists of 180 diagrams.

All integrals of Groups I, II, and III have been evaluated by numerical means. Furthermore, some of them have also been evaluated semianalytically [43]. Group IV integrals have thus far been evaluated only by numerical integration, but in two independent ways, *Version A* and *Version B*, both in Feynman gauge.

The starting point of *Version A* is the RHS of Eq. (14). The algebraic structure of integrals in *Version A* is more complicated than that of *Version B* but their codes are substantially smaller in general than the latter. For Group I, however, there is no advantage of using *Version A*. Thus this group is formulated in *Version B* only.

All integrals are generated from a small number of templates, enabling us to make cross-checking of different diagrams, thereby reducing significantly possible programming errors. More information on *Version A* and *Version B* are given in Appendix A1.

Integrals thus obtained are divergent in general. Since computers are not capable of handling divergence directly, both ultraviolet (UV) and infrared (IR) divergences must be removed beforehand. We have introduced a two-step on shell subtractive renormalization scheme, in which the first step removes both UV and IR divergences but does not give exact on shell results. This is done to circumvent the inconvenient feature of the standard on shell renormalization in which the renormalization terms do not remove and may even introduce extra IR-divergent

terms. The second step yields the standard on shell renormalization result when summed over all diagrams.

The renormalization terms are generated in two ways: One by reduction of the original integral according to a well-defined power-counting rule, and another from scratch, both *analytically*. This enables us to make extensive cross-checking between diagrams of various types and different orders. See Appendix A2 for more details.

All integrals contributing to the α^4 term are evaluated numerically by the adaptive-iterative Monte-Carlo integration routine VEGAS [44]. The major source of numerical uncertainty is the difficulty of accumulating a large number of good sampling points that do not suffer from the *digit-deficiency* problem caused by the round-off error. For this purpose quadruple precision is required in many cases. Unfortunately, this slows down the computation quite drastically. The accuracy of these integrals is checked by comparison with those obtained by other means whenever possible. The results of our calculation are summarized in the following sections. The reliability of these results, which depends critically on the reliability of the numerical integration routine VEGAS, is discussed in Appendix B. Problems caused by nonstatistical errors encountered in dealing with VEGAS and their solution are discussed there in detail.

III. GROUP I DIAGRAMS

Group I diagrams can be classified further into four gauge-invariant subgroups:

Subgroup I(a). Diagrams obtained by inserting three Π_2's (of electron/muon loop) in a second-order muon vertex. Seven Feynman diagrams belong to this subgroup. See Fig. 1(a).

Subgroup I(b). Diagrams obtained by inserting a Π_2 and a Π_4 in a second-order muon vertex. Eighteen Feynman diagrams belong to this subgroup. See Fig. 1(b).

Subgroup I(c). Diagrams containing $\Pi_{4(2)}$. There are nine Feynman diagrams that belong to this subgroup. See Fig. 2.
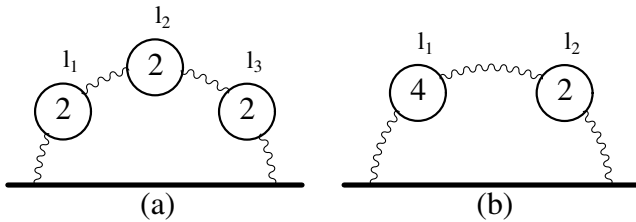

(a)   (b)

FIG. 1.   (a) Diagrams contributing to subgroup I(a). (b) Diagrams contributing to subgroup I(b). Solid horizontal lines represent the muon in external magnetic field. Numerals "2", "4" within solid circles refer to the proper renormalized v-p diagrams Π_2 and Π_4, respectively. Letters l_1, l_2, l_3 refer to electron or muon. Seven and 18 Feynman diagrams contribute to I(a) and I(b), respectively.

Subgroup I(d). Diagrams obtained by insertion of Π_6 in a second-order muon vertex. Fifteen Feynman diagrams belong to this subgroup. Eight are shown in Fig. 3. Diagrams *a, c, d, e, f* and the time-reversed diagram of *e* have charge-conjugated counterparts.

The evaluation of subgroups I(a) and I(b) is greatly facilitated by the analytic formulas available for the second- and fourth-order spectral representations of the renormalized photon propagators [45]. The contribution to a_μ from the diagram obtained by sequential insertion of m kth order electron and n lth order muon v-p loops into a second-order muon vertex is reduced to a simple formula

$$a = \int_0^1 dy(1-y)\left[\int_0^1 ds \frac{\rho_k(s)}{1+\frac{4}{1-s^2}\frac{1-y}{y^2}(\frac{m_e}{m_\mu})^2}\right]^m$$
$$\times \left[\int_0^1 dt \frac{\rho_l(t)}{1+\frac{4}{1-t^2}\frac{1-y}{y^2}}\right]^n, \qquad (18)$$

where ρ_k is the kth order photon spectral function. Exact ρ_2 and ρ_4 can be found in Ref. [45,46]. An exact spectral function for $\Pi_{4(2)}$ and an approximate one for Π_6 are also available [38,47].

The contribution of diagrams of Fig. 1 can be obtained by choosing $(k=2, m=3, n=0), (k=2, m=2, l=2, n=1), (k=2, m=1, l=2, n=2)$. The latest numerical values obtained by evaluating these integrals using VEGAS [44] are listed in Table II, where the number of sampling points per iteration and the number of iterations are also listed.

Note that these diagrams need no additional renormalization. Thus the renormalized amplitudes $a_{2,p2:3}^{(e,e,e)}$, etc., are given by

$$a_{2,p2:3}^{(e,e,e)} = M_{2,p2:3}^{(e,e,e)}, \text{ etc.} \qquad (19)$$

Note also that, to be consistent with notations used later, $M_{2,p2:3}^{(e,e,e)}$, etc., should have been written as $M_{2,p2:3}^{(\mu,e,e,e)}$, etc., The first superscript μ is often (but not always) suppressed for simplicity when there is no danger of confusion.

(a)   (b)

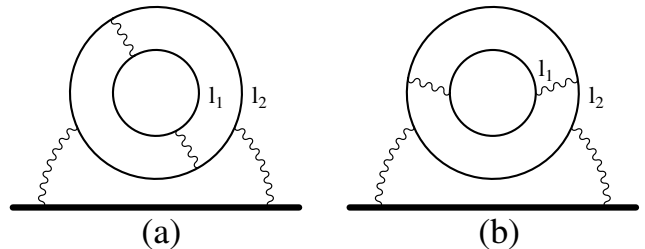FIG. 2.   Diagrams contributing to subgroup I(c). $(l_1, l_2) = (e, e), (e, \mu),$ or (μ, e). See Fig. 1 for notation.
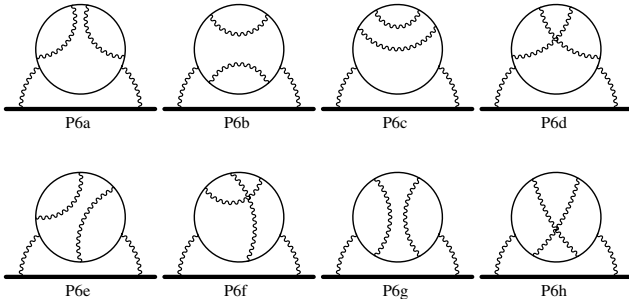
FIG. 3. Eighth-order vertices of subgroup I(d) obtained by insertion of sixth-order (single electron loop) v-p diagram Π_6 in a second-order muon vertex.

Adding up the first three rows of Table II, we obtain the total contribution of diagrams of subgroup I(a)

$$a_{I(a)}^{(8)} = 7.745\,140(30). \tag{20}$$

This is about 40 times more precise than the earlier result [24]. Furthermore it is in excellent agreement with the results obtained by an asymptotic expansion in m_μ/m_e [43]:

$$a_{I(a)}^{(8)}(\text{asymp}) = 7.745\,136\,8(8), \tag{21}$$

where the uncertainty comes only from the measurement of muon mass.

The contributions of Fig. 1(b) for $(l_1, l_2) = (e, e), (e, \mu),$ and (μ, e) can be written down in a similar fashion. The most recent results of numerical integration by VEGAS are listed in the last three rows of Table II. These diagrams need no additional renormalization, too. The sum of these results is the contribution of the subgroup I(b)

$$a_{I(b)}^{(8)} = 7.581\,262(50). \tag{22}$$

This again is in excellent agreement with the asymptotic expansion result [43]

$$a_{I(b)}^{(8)}(\text{asymp}) = 7.581\,275\,5(2), \tag{23}$$

where the uncertainty comes only from the muon mass.

In evaluating the contribution to a_μ from the nine Feynman diagrams of subgroup I(c) shown in Fig. 2, our initial approach was to make use of the parametric integral representation of the v-p term $\Pi_4^{(2)}$. Following the two-step renormalization procedure, these contributions can be written in the form [48].

$$a_{I(c)}^{(8)} = \sum_{(l_1,l_2)} a_{2,P4(P2)}^{(l_1,l_2)}, \tag{24}$$

where each term of

$$a_{2,P4(P2)}^{(l_1,l_2)} = \Delta M_{2,P4a(P2)}^{(l_1,l_2)} + 2\Delta M_{2,P4b(P2)}^{(l_1,l_2)} - 2\Delta B_{2,P2}^{(l_2,l_1)} M_{2,P2}^{(\mu,l_2)}, \tag{25}$$

are finite integrals obtained by the $\mathbf{K}_S$ renormalization procedure described in Ref. [46] and Appendix A. The suffix $P2$ stands for the second-order v-p diagram Π_2, $P4$ for the fourth-order v-p diagram Π_4, while $P4(P2)$ represents the diagram $\Pi_{4(2)}$. $P4$ receives contributions from P_{4a} (vertex correction) and P_{4b} (lepton self-energy insertion), $P4 = P_{4a} + 2P_{4b}$.

The results of numerical evaluation of (25), obtained by VEGAS, are listed in Table III. Numerical values of lower-order Feynman integrals, in terms of which the residual renormalization terms are expressed, are given in Table IV. From these tables and (24) we obtain

$$a_{2,P4(P2)}^{(e,e)} = 1.440\,744(16), \tag{26}$$

$$a_{2,P4(P2)}^{(e,\mu)} = 0.161\,982(11), \tag{27}$$

$$a_{2,P4(P2)}^{(\mu,e)} = 0.021\,583(2). \tag{28}$$

The new results (26) and (28) confirm the old results but with a much higher precision. For (27) the agreement between the old and new values is rather poor.

About a decade ago the leading log term of $a_{2,P4(P2)}^{(e,e)}$ obtained by the renormalization group method [49] seemed to disagree with the numerical evaluation. However, it was found [50] that this was caused by an improper use of the asymptotic photon propagator obtained for massless QED in [51]. It is important to note

TABLE II. Contributions of diagrams of Figs. 1(a) and 1(b). n_F is the number of Feynman diagrams represented by the integral. These evaluations were carried out on α workstations in 2001.

Integral	n_F	Value (Error) including n_F	Sampling per iteration	No. of iterations
$M_{2,P2:3}^{(e,e,e)}$	1	7.223 077 (29)	1×10^9	100
$M_{2,P2:3}^{(\mu,e,e)}$	3	0.494 075 (6)	1×10^8	100
$M_{2,P2:3}^{(\mu,\mu,e)}$	3	0.027 988 (1)	1×10^8	60
$M_{2,P2,P4}^{(e,e)}$	6	7.127 996 (49)	1×10^9	100
$M_{2,P2,P4}^{(\mu,e)}$	6	0.119 601 (3)	1×10^8	60
$M_{2,P2,P4}^{(e,\mu)}$	6	0.333 665 (4)	1×10^8	60

TABLE III.   Contributions of diagrams of Fig. 2. n_F is the number of Feynman diagrams represented by the integral. Numerical work was carried out on α workstations during 2001.

Integral	n_F	Value (Error) including n_F	Sampling per iteration	No. of iterations
$\Delta M_{2,P4a(P2)}^{(e,e)}$	1	0.597 477 1 (111)	1×10^9	100
$\Delta M_{2,P4a(P2)}^{(e,\mu)}$	1	0.121 902 1 (58)	1×10^7	100
$\Delta M_{2,P4a(P2)}^{(\mu,e)}$	1	0.021 017 1 (13)	1×10^7	100
$\Delta M_{2,P4b(P2)}^{(e,e)}$	2	0.982 017 4 (109)	1×10^9	100
$\Delta M_{2,P4b(P2)}^{(e,\mu)}$	2	0.099 244 1 (84)	1×10^7	100
$\Delta M_{2,P4b(P2)}^{(\mu,e)}$	2	0.000 586 0 (4)	1×10^7	100

that the asymptotic photon propagator for massless QED is not the same as one for massive QED as was proven explicitly in [50]. Use of the correct photon propagator in the renormalization group method leads to results which agree very well with the numerical integration result [52,53]. This episode provides an explicit example of danger of confusing the asymptotic behavior with the massless limit, which results in different nonleading terms.

We obtained an independent check of (26) using an exact α^3 spectral function for $\Pi_{4(2)}$ of Fig. 2, which was derived [54] from the QCD spectral function obtained in [47]. Numerical integration using this spectral function gives

$$a_{2,P4(P2)}^{(e,e)} = 1.440\,622(173), \qquad (29)$$

for 100×10^6 sampling points iterated 100 times in quadruple precision. This is in agreement with (26) to the fifth decimal point although their approaches are completely different. Undoubtedly both (26) and (29) must be correct.

The best value of $a_{I(c)}^{(8)}$ is obtained by adding up (26)–(28):

$$a_{I(c)}^{(8)} = 1.624\,308(19). \qquad (30)$$

The contribution to a_μ from 15 diagrams of subgroup I(d) (see Fig. 3) can be written as

TABLE IV.   Auxiliary integrals for Group I. Some integrals are known exactly. Some are obtained by expansion in m_e/m_μ to sufficiently high orders. Their uncertainties come from that of m_e/m_μ only. The remaining integrals are obtained numerically by VEGAS. Total sampling points are of order 10^{11}.

Integral	Value (Error)	Integral	Value (Error)
$M_{2,P2}^{(\mu,e)}$	1.094 258 282 7 (98)	$M_{2,P2}^{(\mu,\mu)}$	0.015 687 421 $\cdots$
$M_{2,P2^*}^{(\mu,e)}$	$-0.161\,084\,05 \cdots$		
ΔB_2	0.75	$\Delta B_{2,P2}^{(e,e)}$	0.063 399 266 $\cdots$
$\Delta B_{2,P2}^{(\mu,e)}$	1.885 732 6 (158)	$\Delta B_{2,P2}^{(e,\mu)}$	9.4055×10^{-6}
ΔL_4	0.465 024 (12)	ΔB_4	$-0.437\,094(21)$
$\Delta \delta m_4$	1.906 340 (22)		

$$a_{2,P6i} = \Delta M_{2,P6i} + \text{residual renormalization terms,}$$
$$(i = a, ..., h). \qquad (31)$$

Divergence-free integrals $\Delta M_{2,P6i}$ are defined by (4.13) of Ref. [46]. Their numerical values (summed over the diagrams related by time-reversal and charge-conjugation symmetries) are evaluated numerically by VEGAS and listed in the third column of Table V.

Summing up the contributions of diagrams a to h of Fig. 3, we obtain the following expression:

$$a_{I(d)}^{(8)} = \sum_{i=a}^{h} \eta_i \Delta M_{2,P6_i} - 4\Delta B_2 \Delta M_{2,P4}^{(\mu,e)} + 5(\Delta B_2)^2 M_{2,P2}^{(\mu,e)}$$
$$- 2(\Delta L_4 + \Delta B_4)M_{2,P2}^{(\mu,e)} - 2\Delta \delta m_4 M_{2,P2^*}^{(\mu,e)}, \qquad (32)$$

where

$$\Delta B_2 = \Delta' B_2 + \Delta' L_2 = \frac{3}{4},$$

$$\Delta M_{2,P4}^{(\mu,e)} = \Delta M_{2,P4a}^{(\mu,e)} + 2\Delta M_{2,P4b}^{(\mu,e)},$$
$$\Delta L_4 = \Delta L_{4x} + 2\Delta L_{4c} + \Delta L_{4l} + 2\Delta L_{4s}, \qquad (33)$$
$$\Delta B_4 = \Delta B_{4a} + \Delta B_{4b},$$
$$\Delta \delta m_4 = \Delta \delta m_{4a} + \Delta \delta m_{4b}.$$

The quantities listed in (33) are defined in Ref. [46]. Their numerical values are listed in Table IV. The 1998 results of numerical integration of $\Delta M_{2,P6i}$ are listed in Table V. From the numerical values in Tables IV and V we obtain the value reported previously [40]:

$$a_{I(d)}^{(8)} = -0.230\,596(416). \qquad (34)$$

This deviates strongly from the old result $-0.7945(202)$ [24]. The problem with [24] was first pointed out in [38] in which $a_{I(d)}^{(8)}$ was evaluated without the $\mathcal{O}(m_e/m_\mu)$ term by a renormalization group method. Soon afterwards a Padé approximant of the sixth-order photon spectral function was used to evaluate the full correction [55]:

$$a_{I(d)}^{(8)}(\text{Padé}) = -0.230\,362(5). \qquad (35)$$

Our new result (34) is in good agreement with (35). The

TABLE V.   Contributions of diagrams of Fig. 3. n_F is the number of Feynman diagrams represented by the integral. $M_{2,P6e}$ was evaluated in 1998 on SP2 at Cornell Theory Center. Others were evaluated in 1998 on Fujitsu VX at Nara Women's University, Japan.

Integral	n_F	Value (Error) including n_F	Sampling per iteration	No. of iterations
$\Delta M_{2,P6a}$	2	5.676 002 (168)	4×10^8	60
$\Delta M_{2,P6b}$	1	3.058 301 (152)	2×10^8	60
$\Delta M_{2,P6c}$	2	1.483 501 (104)	2×10^8	60
$\Delta M_{2,P6d}$	2	$-3.127 282(122)$	2×10^8	60
$\Delta M_{2,P6e}$	4	$-0.073 885(234)$	6×10^8	60
$\Delta M_{2,P6f}$	2	$-4.064 113(151)$	2×10^8	60
$\Delta M_{2,P6g}$	1	$-0.247 237(100)$	2×10^8	60
$\Delta M_{2,P6h}$	1	2.838 657 (74)	2×10^8	60

primary cause of the old discrepancy was traced to very poor statistics of the original evaluation [56]. Increase of statistics by 2 orders of magnitude improved the result to $-0.2415(19)$ [39]. However, the discrepancy with (35) was still non-negligible. Finally, the problem was traced to round-off errors caused by insufficient number of effective digits in real*8 arithmetic in carrying out renormalization by numerical means [40]. This was resolved by going over to the real*16 arithmetic. (See Appendix B for further discussion on this point.)

Note that the uncertainty in (35) may be an underestimate since it does not include the uncertainty of the Padé approximation itself. However, it seems to be small compared with the quoted uncertainty [40]. In principle it is possible to prove or disprove it by more numerical work. However, it would require 6000 times more computing time in order to match the precision of (35) achieved by the Padé method. This is not only impractical but also pointless since there is no need to improve the current precision further.

Collecting the results (21), (23), (30), and (35), we find the best value of the contribution to the muon anomaly from the 49 diagrams of group I:

$$a_I^{(8)} = 16.720 359(20). \qquad (36)$$

IV. GROUP II DIAGRAMS

Diagrams of this group are generated by inserting Π_2 and Π_4 in the photon lines of fourth-order muon vertex diagrams. Use of analytic expressions for the second- and fourth-order spectral functions for the photon propagators and time-reversal symmetry cuts down the number of independent integrals in *Version A* from 90 to 11.

The contribution to a_μ arising from the set of vertex diagrams represented by the "self-energy" diagrams of Fig. 4 can be written in the form

$$a_{4,P_\alpha} = \Delta M_{4,P_\alpha} + \text{residual renormalization terms}, \quad (37)$$

where $\Delta M_{4,P_\alpha}$ are finite integrals obtained in the intermediate step of two-step renormalization [57]. Their

numerical values, obtained by VEGAS are listed in Table VI. The values of auxiliary integrals needed to calculate the total contribution of group II diagrams are given in Tables IV and VII.

Summing the contributions of diagrams of the first, second, and third rows of Fig. 4, one obtains

$$a_{4,P4} = 2\Delta M_{4a,P4}^{(\mu,e)} + \Delta M_{4b,P1':4}^{(\mu,e)} + \Delta M_{4b,P0:4}^{(\mu,e)}$$
$$- \Delta B_2 M_{2,P4}^{(\mu,e)} - \Delta B_{2,P4}^{(\mu,e)} M_2, \qquad (38)$$

$$a_{4,P2,P2} = \Delta M_{4a,P2,P2}^{(e,e)} + \Delta M_{4b,P1':2,P0:2}^{(e,e)} - \Delta B_{2,P2}^{(\mu,e)} M_{2,P2}^{(\mu,e)}$$
$$+ 2\Delta M_{4a,P2,P2}^{(e,\mu)} + \Delta M_{4b,P1':2,P0:2}^{(e,\mu)} + \Delta M_{4b,P1':2,P0:2}^{(\mu,e)}$$
$$- \Delta B_{2,P2}^{(\mu,e)} M_{2,P2}^{(\mu,e)} - \Delta B_{2,P2}^{(\mu,e)} M_{2,P2}^{(\mu,\mu)}, \qquad (39)$$

$$a_{4,P2:2} = 2\Delta M_{4a,P2:2}^{(e,e)} + \Delta M_{4b,P1':2:2}^{(e,e)} + \Delta M_{4b,P0:2:2}^{(e,e)}$$
$$- \Delta B_2 M_{2,P2:2}^{(e,e)} - \Delta B_{2,P2:2}^{(e,e)} M_2 + 4\Delta M_{4a,P2:2}^{(e,\mu)}$$
$$+ 2\Delta M_{4b,P1':2:2}^{(e,\mu)} + 2\Delta M_{4b,P0:2:2}^{(e,\mu)} - 2\Delta B_2 M_{2,P2:2}^{(e,\mu)}$$
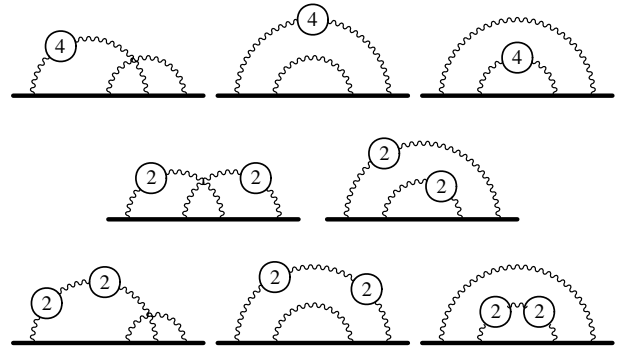$$- 2\Delta B_{2,P2:2}^{(e,\mu)} M_2, \qquad (40)$$

FIG. 4.   Eighth-order diagrams obtained from the fourth-order vertex diagrams by inserting vacuum-polarization loops Π_2 and Π_4, which consist of either electron or muon loop.

TABLE VI.   Contributions of diagrams of Fig. 4. n_F is the number of Feynman diagrams represented by the integral. t.r. refers to time-reversed amplitude. Numerical evaluation was carried out on α workstations in 2001.

Integral	n_F	Value (Error) including n_F	Sampling per iteration	No. of iterations
$\Delta M_{4a,P4}^{(\mu,e)}$ + t.r.	18	2.047 838 (221)	1×10^9	100
$\Delta M_{4b,P0:4}^{(\mu,e)} + \Delta M_{4b,P1':4}^{(\mu,e)}$	18	$-2.486\,595(119)$	1×10^9	120
$\Delta M_{4a,P2,P2}^{(e,e)}$ + t.r.	3	2.289 959 (144)	1×10^9	100
$\Delta M_{4a,P2,P2}^{(e,\mu)}$ + t.r.	6	0.054 120(34)	1×10^8	100
$\Delta M_{4b,P1':2,P0:2}^{(e,e)}$	3	$-4.249\,598(76)$	1×10^9	100
$\Delta M_{4b,P1':2,P0:2}^{(\mu,e)} + \Delta M_{4b,P1':2,P0:2}^{(e,\mu)}$	6	$-0.485\,108(14)$	1×10^8	100
$\Delta M_{4a,P2:2}^{(e,e)}$ + t.r.	6	5.148 441(377)	1×10^9	100
$\Delta M_{4a,P2:2}^{(e,\mu)}$ + t.r.	12	0.260 977(103)	1×10^8	100
$\Delta M_{4b,P0:2:2}^{(e,e)} + \Delta M_{4b,P1':2:2}^{(e,e)}$	6	$-8.633\,608(190)$	1×10^9	100
$\Delta M_{4b,P0:2:2}^{(e,\mu)} + \Delta M_{4b,P1':2:2}^{(e,\mu)}$	12	$-1.102\,819(42)$	1×10^8	100

respectively, where $M_{2,P4}^{(\mu,e)}$ is equal to $\Delta M_{2,P4}^{(\mu,e)} - 2\Delta B_2 M_{2,P2}^{(\mu,e)}$. The factor two in front of $\Delta M_{4a,\ldots}$ accounts for equivalent diagrams obtained by time-reversal and another factor two in front of $\Delta M_{4a,\ldots}$ and $\Delta M_{4b,\ldots}$ accounts for interchange of electron and muon vacuum-polarization loops. In contrast, the auxiliary integrals listed in Tables IV and VII do not include multiplicity. Following the convention adopted below Eq. (19), the first superscript μ indicating the external muon line is suppressed for simplicity. For instance, $\Delta M_{4a,P2,P2}^{(\mu,e,e)}$ is written as $\Delta M_{4a,P2,P2}^{(e,e)}$.

Substituting the data from Tables IV and VI into (38)–(40), we obtain

$$a_{4,P4} = -2.778\,565(253),$$
$$a_{4,P2,P2} = -4.553\,017(68), \tag{41}$$
$$a_{4,P2:2} = -9.342\,599(438).$$

Two of these terms were also evaluated in [43] by an asymptotic expansion in m_μ/m_e:

$$a_{4,P4}(\text{asymp}) = -2.778\,852\,33(5),$$
$$a_{4,P2:2}(\text{asymp}) = -9.342\,722\,1(5). \tag{42}$$

They are in excellent agreement with the numerical integration results.

TABLE VII.   Auxiliary integrals for Group II. Some integrals are known exactly. Some are obtained by expansion in m_e/m_μ to necessary orders. Their uncertainties come from that of m_e/m_μ only. Remaining integrals are obtained by VEGAS integration, with total sampling points of order 10^{11}.

Integral	Value (Error)	Integral	Value (Error)
M_2	0.5	$M_{2,P4}^{(\mu,e)}$	1.493 671 581 (8)
$M_{2,P2:2}^{(e,e)}$	2.718 655 7 (1)	$M_{2,P2:2}^{(\mu,e)}$	0.050 259 648 (1)
ΔB_2	0.75	$\Delta B_{2,P2}^{(\mu,\mu)}$	0.063 399 266 $\cdots$
$\Delta B_{2,P2:2}^{(e,e)}$	5.330 381 (61)	$\Delta B_{2,P2:2}^{(e,\mu)}$	0.236 018 (9)
$\Delta B_{2,P4}^{(\mu,e)}$	2.439 109 (53)		

Combining the results (42) and the value of $a_{4,P2,P2}$ from (41) we find the best value for the contribution of 90 diagrams of group II to be

$$a_{II}^{(8)} = -16.674\,591(68). \tag{43}$$

V. GROUP III DIAGRAMS

Diagrams belonging to this group are generated by inserting a second-order vacuum-polarization loop Π_2 in the photon lines of sixth-order muon vertex diagrams of the three-photon-exchange type. Time-reversal invariance and use of the function ρ_2 [see (18)] for the photon spectral function reduce the number of independent integrals in *Version A* from 150 to 8. Some of these integrals are represented by the "self-energy" diagrams of Fig. 5.

Let $M_{6\alpha,P}$ be the magnetic moment projection in *Version A* of the set of 150 diagrams generated from a self-energy diagram α ($= A$ through H) of Fig. 5 by insertion of Π_2 and an external-vertex. The renormalized contribution due to the group III diagrams can then be written as

$$a_{III}^{(8)} = \sum_{\alpha=A}^{H} \eta_\alpha a_{6\alpha,P2}, \tag{44}$$

where

$$a_{6\alpha,P2} = \Delta M_{6\alpha,P2} + \text{residual renormalization terms.} \tag{45}$$
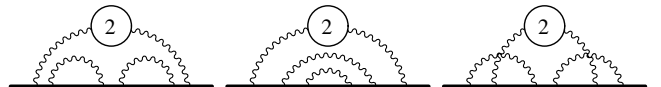

FIG. 5.   Typical eighth-order diagrams obtained by insertion of a vacuum-polarization loop Π_2 in muon diagrams of the three-photon-exchange type. Altogether there are 150 diagrams of this type.

where all divergences have been projected out by $\mathbf{K}_S$ and $\mathbf{I}_R$ operations. (See Ref. [57].)

The latest numerical values of Group III integrals are summarized in Table VIII. Numerical values of auxiliary integrals needed in the renormalization scheme are listed in Tables IV, VII, and IX. For comparison, the results of old calculation [24] carried out in double precision are listed in the last column of Table VIII. This is to examine the effect of *digit-deficiency* error. In this case the effect is relatively mild because the introduction of a vacuum-polarization loop tends to make the integrand less sensitive to the singularity.

When summed over all the diagrams of group III, the UV- and IR-divergent pieces cancel out and the total contribution to a_μ can be written as a sum of finite pieces:

$$
\begin{aligned}
a_{III}^{(8)} = &\sum_{\alpha=A}^{H} \eta_\alpha \Delta M_{6\alpha,P2} - 3\Delta B_{2,P2}^{(\mu,e)}\Delta M_4 - 3\Delta B_2 \Delta M_{4,P2}^{(\mu,e)} \\
&+ (M_{2^*,P2}^{(\mu,e)}[I] - M_{2^*,P2}^{(\mu,e)})\Delta\delta m_4 + (M_{2^*}[I] - M_{2^*}) \\
&\times \Delta\delta m_{4,P2}^{(\mu,e)} - M_{2,P2}^{(\mu,e)}[\Delta B_4 + 2\Delta L_4 - 2(\Delta B_2)^2] \\
&- M_2(\Delta B_{4,P2}^{(\mu,e)} + 2\Delta L_{4,P2}^{(\mu,e)} - 4\Delta B_2 \Delta B_{2,P2}^{(\mu,e)}). \quad (46)
\end{aligned}
$$

Plugging the values listed in Tables IV, VII, and IX in (46), we obtain

$$
a_{III}^{(8)} = 10.793\,43(414). \quad (47)
$$

The error in (47) can be reduced easily if necessary. The ration $a_{III}^{(8)}/\tilde{a}^{(6)}$, where $\tilde{a}^{(6)}$ is the value of sixth-order muon moment without closed lepton loop, is about 11, which is not very far from the very crude expectation $3K \sim 9$, where K is from (68), although such a comparison is more appropriate for individual terms on Table VIII than their sum. See Sec. VIII for further discussion of enhancement factor K.

VI. GROUP IV DIAGRAMS

Diagrams of this group can be divided into four subgroups: IV(a), IV(b), IV(c), and IV(d). Each subgroup

TABLE IX. Auxiliary integrals for Group III. Some integrals are known exactly. Some are obtained by expansion in m_e/m_μ to necessary orders. Their uncertainties come from that of m_e/m_μ only. Remaining integrals are obtained by VEGAS integration, with total sampling points of order 10^{11}.

Integral	Value (Error)	Integral	Value (Error)
M_{2^*}	1.0	$M_{2^*}[I]$	-1.0
$M_{2^*,P2}^{(\mu,e)}$	2.349 621 (35)	$M_{2^*,P2}^{(\mu,e)}[I]$	$-2.183\,159(95)$
ΔM_4	$0.030833612\cdots$	$\Delta M_{4,P2}^{(\mu,e)}$	$-0.628\,831\,80(2)$
$\Delta L_{4,P2}^{(\mu,e)}$	3.118 868 (201)	$\Delta B_{4,P2}^{(\mu,e)}$	$-3.427\,615(237)$
$\Delta\delta m_4$	1.906 340 (22)	$\Delta\delta m_{4,P2}^{(\mu,e)}$	11.151 387 (303)

consists of two equivalent sets of diagrams related by charge-conjugation (reversal of the direction of momentum flow in the loop of the light-by-light scattering subdiagram). Diagrams of subgroups IV(a), IV(b), and IV(c) are obtained by modifying the sixth-order diagram which contains the light-by-light scattering subdiagram Λ_4, one of whose external photon line represents the magnetic field. The magnetic moment contribution M_{6LL} of this sixth-order diagram is known analytically [34], whose numerical value is

$$
M_{6LL} = 20.947\,924\,34(21) \quad (48)
$$

when Λ_4 is an electron loop, and the uncertainty is due to that of the muon mass only.

Subgroup IV(a). Diagrams obtained by inserting a second-order vacuum-polarization loop Π_2 in M_{6LL}. They are all appropriate modifications of the integral $M_{6LL,P2}$ defined by (2.4) of Ref. [58]. Denote these integrals as $M_{6LL,P2}^{(l_1,l_2)}$ where $(l_1, l_2) = (e, e), (e, \mu)$ or (μ, e). This subgroup is comprised of 54 diagrams. They are generically represented by the self-energy-like diagrams shown in Fig. 6.

Subgroup IV(b). Diagrams containing sixth-order light-by-light scattering subdiagrams Λ_6. Altogether, there are 60 diagrams of this type. Charge-conjugation and time-reversal symmetries and summation over external-vertex insertions reduce the number of inde-

TABLE VIII. Contributions of diagrams of Fig. 5. n_F is the number of Feynman diagrams represented by the integral. This calculation was carried out in quadruple precision in 2001 - 2003 on α workstations to examine the influence of *digit-deficiency* error in the calculation of [24] carried out in double precision.

| Integral	n_F	Value (Error) including n_F	Sampling per iteration	No. of iterations	Data from Ref. [24]
$\Delta M_{6a,P2}$	15	$-12.934\,780(1081)$	4×10^8	100	$-12.9401(130)$
$\Delta M_{6b,P2}$	15	18.797 294 (1309)	4×10^8	140	18.7970 (171)
$\Delta M_{6c,P2}$	15	3.997 996 (1773)	4×10^8	100	4.0007 (178)
$\Delta M_{6d,P2}$	30	10.492 627 (1507)	8×10^8	111	10.4940 (225)
$\Delta M_{6e,P2}$	15	10.990 435 (981)	4×10^8	119	11.0001 (121)
$\Delta M_{6f,P2}$	15	5.652 451 (1503)	4×10^8	100	5.6518 (166)
$\Delta M_{6g,P2}$	30	19.747 805 (1558)	4×10^8	100	19.7424 (172)
$\Delta M_{6h,P2}$	15	$-18.363\,491(1433)$	4×10^8	100	$-18.3615(141)$
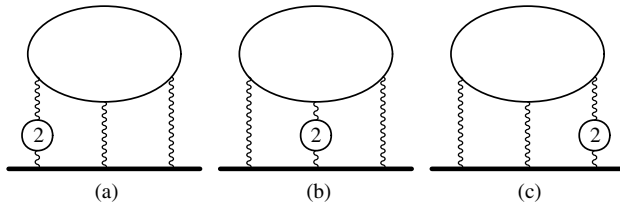
FIG. 6.   Muon self-energy-like diagrams representing the external-vertex-summed integrals of subgroup IV(a). $(l_1, l_2) = (e, e), (e, \mu)$, or (μ, e), where l_1, l_2 refer to the light-by-light scattering loop Λ_4 and vacuum-polarization loop Π_2, respectively.

pendent integrals to four in *Version A*. These integrals are generically represented by the self-energy-like diagrams LLA, LLB, LLC and LLD of Fig. 7.

Subgroup IV(c). Diagrams obtained by including second-order radiative corrections on the muon line of M_{6LL}. There are 48 diagrams that belong to this subgroup. Summation over external-vertex insertions and use of the interrelations available due to charge-conjugation and time-reversal symmetries leave five independent integrals in *Version A*. They are generically represented by the self-energy-like diagrams LLE, LLF, LLG, LLH and LLI of Fig. 7.

Subgroup IV(d). Diagrams generated by inserting Λ_4 *internally* in fourth-order vertex diagrams. Diagrams of this type appear for the first time in the eighth-order. Charge-conjugation invariance and summation over the external-vertex insertion with the help of the Ward-Takahashi identity lead us to three independent integrals in *Version A*. They are represented by the diagrams LLJ, LLK and LLL of Fig. 7. No further discussion of this subgroup will be given in this paper since it was treated in a separate paper [23].
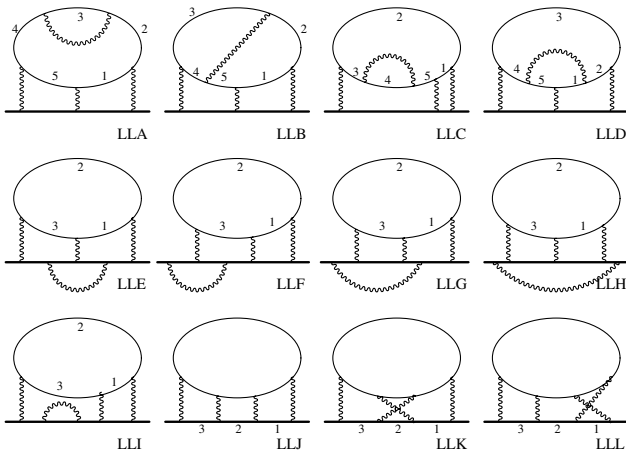

FIG. 7.   Muon self-energy-like diagrams representing (external-vertex-summed) integrals of subgroup IV(b), IV(c), and IV(d).

In subgroups IV(a), IV(b), and IV(c) UV-divergences arising from the light-by-light scattering subdiagram Λ_4, or more explicitly $\Pi^{\nu\alpha\beta\gamma}(q, k_i, k_j, k_l)$, can be taken care of by making use of the identity:

$$\Pi^{\nu\alpha\beta\gamma}(q, k_i, k_j, k_l) = -q_\mu\left[\frac{\partial}{\partial q_\nu}\Pi^{\mu\alpha\beta\gamma}(q, k_i, k_j, k_l)\right],$$
$$(49)$$

which follows from the Ward-Takahashi identity. Namely, no explicit UV renormalization is needed if one uses the RHS of (49) instead of the LHS and the fact that $\Sigma(p)$ of (14) vanishes by Furry's theorem. On the other hand, $\Sigma(p)$ is nonzero for subgroup IV(d) and the UV-divergence associated with the light-by-light scattering subdiagram Λ_4 must be regularized, e.g., by dimensional regularization. For these diagrams it is necessary to carry out explicit renormalization of Λ_4 as well as that of the two sixth-order vertex subdiagrams containing Λ_4. See [23] for a detailed discussion of renormalization based on a combination of dimensional regularization and Pauli-Villars regularization.

As was announced in Sec. I, all diagrams of Group IV have now been evaluated in both *Version A* and *Version B*. In the following let us consider *Version A* and *Version B* separately since renormalization is handled slightly differently in two cases.

A. Version A

The calculation of group IV(a) contribution is particularly simple. This is because M_{6LL} has been fully tested by comparison with the analytic result [34], and insertion of the vacuum-polarization term is straightforward. One therefore finds that integrals $M_{6LL,P2}^{(l_1,l_2)}$ are all finite, which means

$$a_{6LL,P2}^{(l_1,l_2)} = M_{6LL,P2}^{(l_1,l_2)} = \Delta M_{6LL,P2}^{(l_1,l_2)},\qquad(50)$$

where l_1, l_2 refer to the light-by-light scattering loop Λ_4 and vacuum-polarization loop Π_2, respectively. Thus the contribution of subgroup IV(a) can be written as

$$a_{IV(a)}^{(8)} = \sum_{(l_1,l_2)} \Delta M_{6LL,P2}^{(l_1,l_2)},\qquad(51)$$

where the individual terms are given in Table X.

Let us denote magnetic projections of subgroups IV(b) and IV(c) as $M_{8LL\alpha}$ where $\alpha = A, .., I$. Relating the IR- and UV-divergent $M_{8LL\alpha}$ to the finite, numerically calculable piece $\Delta M_{8LL\alpha}$ defined by the procedure of two-step renormalization of Ref. [58], one can write the contributions of the diagrams of subgroups IV(b) and IV(c) as

$$a_{IV(b)}^{(8)} = \sum_{\alpha=A}^{D} \eta_\alpha \Delta M_{8LL\alpha} - 3\Delta B_2 M_{6LL},\qquad(52)$$

TABLE X. Contributions of diagrams of Fig. 6. n_F is the number of Feynman diagrams represented by the integral. The main term $\Delta M_{6LL,P2}^{(e,e)}$ was evaluated on $\nu 1$ at Cornell Theory Center in 2001. The rest were evaluated in 2001 on Condor cluster at University of Wisconsin.

Integral	n_F	Value (Error) including n_F	Sampling per iteration	No. of iteration
$\Delta M_{6LL,P2}^{(e,e)}$	18	116.759 183 (292)	6×10^{10}	180
$\Delta M_{6LL,P2}^{(e,\mu)}$	18	2.697 443 (142)	1×10^{8}	110
$\Delta M_{6LL,P2}^{(\mu,e)}$	18	4.328 885 (293)	1×10^{9}	100

and

$$a_{IV(c)}^{(8)} = \sum_{\alpha=E}^{I} \eta_\alpha \Delta M_{8LL\alpha} - 2\Delta B_2 M_{6LL}. \qquad (53)$$

Numerical integration of all terms contributing to $a_{IV}^{(8)}$ has been carried out using VEGAS [44]. The latest results for Groups IV(b) and IV(c) are listed in Table XI. The result for Group IV(d) had been handled separately [23]. In general, the major difficulty in dealing with the diagrams of Groups IV(b) and IV(c) arises from the enormous size of integrands (up to 5000 terms and 240 kilobytes of FORTRAN source code per integral) and the large number of integration variables (up to 10).

Diagrams of Groups IV(b) and IV(c) have singular surfaces just outside of the integration domain (unit cube) at a distance of $\sim (m_e/m_\mu)^2 \sim 1/40\,000$. This makes the evaluation of their contributions to $A_2^{(8)}(m_\mu/m_e)$ much more sensitive to the d-d problem

compared with the evaluation of the same set of diagrams contributing to the mass-independent $A_1^{(8)}$ whose singularity is far outside (~ 1) of the domain of integration.

Because of the d-d problem intensified by the proximity of the singularity, all strategies discussed in Appendix B had to be tried to evaluate these integrals.

In most cases the first step is to make the integrand smoother by *stretching* (see Appendix B), which is repeated several times until the integrand behaves more gently.

Although *chopping* (see Appendix B) was handy to obtain a rough estimate quickly, we had to abandon it in the end because extrapolation to $\delta = 0$ turned out to be too unreliable in order to reach the desired precision.

Most integrals were then evaluated by *splitting* them into two parts, one evaluated in real*8 and the other in real*16. In some cases, however, even the part evaluated in real*16 suffered from a severe d-d problem, preventing us from collecting large enough samplings for high statistics. Analyzing this problem closely, we found that it is possible to evaluate these integrals by the following procedure: First try several iterations with a positive rescale parameter β (typically $\beta = 0.5$) until VEGAS begins to show strong sign of blowing up due to the d-d problem. Then *freeze* β to 0 (see Appendix B). This may solve the problem in most cases. If not, try several iterations and see how rapidly the calculation runs into the d-d problem. It turns out that it takes place very early if we chose too many sampling points N_S per iteration. This is because choosing large N_S increases the chance of hitting random numbers too close to the singularity within one iteration.

TABLE XI. Contributions of diagrams of Fig. 7 excluding LLJ, LLK, and LLL which were evaluated separately in Ref. [23]. n_F is the number of Feynman diagrams represented by the integral. Some integrals are split into two parts: *d-part* is evaluated in real*8 and *q-part* is evaluated in real*16. *a-part* refers to the adjustable precision method developed by [42]. The superscript $*$ indicates that indicated contributions were obtained by extrapolation from calculations in which the edges of integration domain were chopped off by 1.d-10. See Appendix B for details. Numerical work was carried out on SP3, velocity cluster, SP2, Condor cluster, and α workstations over several years. The table lists only the latest of results obtained by various means.

Integral	n_F	Value (Error) including n_F	Sampling per iteration	No. of iterations
ΔM_{8LLA}	10	52.063 459 (1497)	4×10^{8}	3300
ΔM_{8LLB}	20	$-75.014\,508(1838)$		
d-part		$-53.000\,600(981)$	1×10^{10}	430
*a-part**		$-22.013\,908(1554)$	4×10^{7}	460
ΔM_{8LLC}	20	107.488 810 (2811)	4×10^{8}	5900
ΔM_{8LLD}	10	$-37.824\,352(1137)$	1×10^{10}	200
ΔM_{8LLE}	6	$-21.607\,656(1053)$		
d-part		$-20.920\,745(446)$	1×10^{10}	304
a-part		$-0.686\,911(954)$	2×10^{7}	280
ΔM_{8LLF}	12	$-75.766\,143(2223)$	1×10^{10}	1000
ΔM_{8LLG}	12	$-35.077\,389(1410)$	1×10^{10}	470
ΔM_{8LLH}	6	54.025 704 (2411)		
d-part		51.820 951 (889)	2×10^{10}	470
*q-part**		2.204 753 (2241)	4×10^{7}	391
ΔM_{8LLI}	12	112.756 785 (2683)	1×10^{10}	450

As a consequence the *d-d* problem is likely to dominate each iteration and makes it very difficult to collect a large enough number of good samplings. We found that a better strategy is to reduce the size of N_S to a moderate value and, instead, increase the number of iterations N_I substantially. This is acceptable since, for $\beta = 0$ which means that the distribution function ρ is no longer changed from iteration to iteration, the final error generated by VEGAS depends only on the product $N_S N_I$.

This strategy has been applied, in particular, to the diagrams LLA and LLC, as is seen from Table XI. Entries in Table XI are only the best of results obtained by various methods discussed above. They are consistent with each other despite their diverse approaches.

One obtains from Tables X and XI the contributions of subgroup IV(a) and the *Version A* contributions of subgroups IV(b) and IV(c):

$$a_{IV(a)}^{(8)} = 123.785\,51(44),$$
$$a_{IV(b)}^{(8)} = -0.419\,42(385), \tag{54}$$
$$a_{IV(c)}^{(8)} = 2.909\,41(459).$$

B. Version B

In *Version B* the magnetic moment projection is evaluated for each vertex diagram on the LHS of (14). It is convenient to denote these diagrams in terms of self-energy-like diagrams of Fig. 7, by attaching suffix i to indicate the lepton line in which an external magnetic field vertex is inserted. For instance, we obtain vertex diagrams LLA1, LLA2, ..., LLA5 from the diagram LLA.

We will not discuss subgroup IV(a) here since its *Version A* has already been fully tested. For subgroup IV(b) we find

$$a_{IV(b)}^{(8)} = \sum_{\alpha=A}^{D} \sum_{i=1}^{5} \eta_\alpha \Delta M_{8LL\alpha i} - 4\Delta B_2 M_{6LL}, \tag{55}$$

instead of (52). Note that the last term of (55) is different from that of (52). This is not an error. It arises from difference in the definition of ΔM terms.

Similarly, for subgroup IV(c) we obtain

$$a_{IV(c)}^{(8)} = \sum_{\alpha=E}^{I} \sum_{i=1}^{3} \eta_\alpha \Delta M_{8LL\alpha i} - 2\Delta B_2 M_{6LL}. \tag{56}$$

The results of numerical evaluation are listed in Table XII. Precision of these calculations is still modest but high enough to show the consistency with the calculation of *Version A*. See the last column of Table XII for comparison of two Versions. Numerical work has been carried out with the same care as that described for *Version A*. The numerical calculation of ΔM_{8LLB} was particularly difficult.

One obtains from Table XII the values of $a_{IV(b)}^{(8)}$ and $a_{IV(c)}^{(8)}$

$$a_{IV(b)}^{(8)} = -0.3720(168),$$
$$a_{IV(c)}^{(8)} = 2.8763(173), \tag{57}$$

which are not inconsistent with those given in (54), although much improvement is needed to become competitive with the *Version A* results.

C. Total contribution of Group IV

The contribution of subgroup IV(a) is listed only in (54) since it was not evaluated in *Version B*. The statistical combination of two versions of subgroups IV(b) and IV(c) is dominated by *Version A* since *Version B* still does not

TABLE XII.   Contribution of Group IV(b) and Group IV(c) diagrams of Fig. 7 evaluated in *Version B*. Double precision is used for all calculations which are carried out on Fujitsu VPP at RIKEN. Finite renormalization terms $\Delta B_2 M_{6LLi}$, $i = 1, 2, 3$, are needed for LLA and LLC, respectively, in order to compare them with the calculations in *Version A*. $M_{6LL(2+3)} \equiv M_{6LL2} + M_{6LL3}$ is obtained subtracting M_{6LL1} from the known value of $M_{6LL}(\equiv M_{6LL1} + M_{6LL2} + M_{6LL3})$ given in (48).

Integral	n_F	Value (Error) including n_F	Sampling per iteration	No. of iterations	Difference *Ver.A* - *Ver.B*
ΔM_{8LLA}	10	52.080\,79 (731)			$-0.017\,33(746)$
$\sum_{i=1}^{5} \eta_A \Delta M_{8LLAi}$		60.467\,98 (731)	1×10^9	122	
$-\Delta B_2 M_{6LL2}$		$-8.387\,20(15)$	1×10^{10}	280	
ΔM_{8LLB}	20	$-74.999\,66(1060)$	1×10^9	544	$-0.014\,85(1075)$
ΔM_{8LLC}	20	107.503\,69 (877)			$-0.014\,88(920)$
$\sum_{i=1}^{5} \eta_C \Delta M_{8LLCi}$		114.827\,43 (876)	1×10^9	357	
$-\Delta B_2 M_{6LL(1+3)}$		$-7.323\,75(15)$			
ΔM_{8LLD}	10	$-37.823\,98(580)$	1×10^9	120	$-0.000\,37(591)$
ΔM_{8LLE}	6	$-21.611\,47(562)$	1×10^9	120	$+0.003\,81(571)$
ΔM_{8LLF}	12	$-75.778\,67(855)$	1×10^9	431	$+0.012\,53(883)$
ΔM_{8LLG}	12	$-35.074\,71(683)$	1×10^9	120	$-0.00268(697)$
ΔM_{8LLH}	6	54.013\,78 (619)	1×10^9	262	$+0.01192(664)$
ΔM_{8LLI}	12	112.749\,26 (1037)	1×10^9	512	$+0.00752(1071)$

have large statistics. Only subgroup IV(d) has been evaluated in both versions with comparable statistical weights [23]. Our best results for the gauge-invariant subgroups of group IV can be summarized as

$$a_{IV(a)}^{(8)} = 123.785\,51(44), \qquad a_{IV(b)}^{(8)} = -0.417\,04(375),$$

$$a_{IV(c)}^{(8)} = 2.907\,22(444), \qquad a_{IV(d)}^{(8)} = -4.432\,43(58), \qquad (58)$$

where $a_{IV(b)}^{(8)}$, $a_{IV(c)}^{(8)}$, and $a_{IV(d)}^{(8)}$ are statistical combinations of *Version A* and *Version B*.

Summing up these terms one find that the contribution from all 180 diagrams of group IV is given by

$$a_{IV}^{(8)} = 121.8431(59). \qquad (59)$$

Finally, combining (36) with (43), (47), and (60), one obtains the value given in (15).

VII. EVALUATION OF $A_3^{(8)}(m_\mu/m_e, m_\mu/m_\tau)$

There is a small contribution to a_μ from the three-mass term $A_3^{(8)}(m_\mu/m_e, m_\mu/m_\tau)$ which arises from 102 diagrams containing at least two closed fermion loops, of v-p and/or l-l type. The contribution of 30 diagrams analogous to those of Fig. 1 and 2 is

$$A_{3I}^{(8)}(m_\mu/m_e, m_\mu/m_\tau) = 0.007\,630(1). \qquad (60)$$

The contribution of 36 diagrams related to those of Fig. 4 is

$$A_{3II}^{(8)}(m_\mu/m_e, m_\mu/m_\tau) = -0.053\,818(37). \qquad (61)$$

The contribution of 36 diagrams analogous to those of Fig. 6 is

$$A_{3IV}^{(8)}(m_\mu/m_e, m_\mu/m_\tau) = 0.083\,782(75). \qquad (62)$$

Summation of these results leads to the value given in (17). The value 0.079 (3) quoted in [24] is in rough agreement with (62). In [24] it was assumed that the only nontrivial contribution to the eighth-order term arises from a muon vertex that contains an electron light-by-light scattering subdiagram and a tau vacuum-polarization loop and another in which the roles of electron and tau are interchanged. [See Fig. 6 with $(l_1, l_2) = (e, \tau), (\tau, e)$.] It did not include the contributions (60) and (61). Our new calculation shows that this assumption was not justified. This is presumably because the mechanism that makes M_{6LL} enhanced (see discussion in Sec. VIII) does not work if the momenta of photons exchanged between muon and electron are not very small.

Another term of order α^4 is $A_2^{(8)}(m_\mu/m_\tau)$ which is calculable from 469 Feynman diagrams. However, its contribution to a_μ is of the order $(m_\mu/m_\tau)^2 \times \ln(m_\tau/m_\mu)A_2^{(8)}(1) \sim 0.005$ so that it may be safely ignored without actual calculation.

VIII. DISCUSSION

The size of integrals belonging to Groups I and II is rather small. Thus they have been evaluated using a large number of sampling points, achieving precision of five or more digits. Furthermore, most of these integrals have been evaluated in alternative ways, either analytic or semianalytic. The agreement between numerical and (semi) analytic calculations is so precise that it leaves no room for questioning the results.

A similar comment applies to the integrals of Group III and Group IV(a), which are obtained by insertion of a vacuum-polarization loop Π_2 in the corresponding sixth-order diagrams, which have been fully tested against the analytic integration results.

For the integrals of Group IV(d) formulation in *Version B* enabled us to discover an error in the *Version A*. After correcting the error, we now have two independent calculations which give the same results. For the remaining diagrams, of Groups IV(b) and IV(c), their structure had been tested extensively taking advantage of the fact that they have in general vertex and/or self-energy subtraction terms, which can be generated in two ways: One from a well-defined reduction procedure of the original unrenormalized integral, and another by construction of the renormalization terms from scratch, *both analytically*. The agreement of these two, proof of which often requires nontrivial analytic work, give a strong confirmation of their structure and of the master program from which all eighth-order integrals of individual diagrams is derived. See Appendix A2 for details.

In order to obtain a further and definitive check, however, we have constructed IV(b) and IV(c) in *Version B*, too. As a consequence, we have integrands of Groups IV(b) and IV(c) in two versions. Extensive numerical work has shown that they are consistent with each other within the error bars of computation. This completes a comprehensive check of all diagrams contributing to $A_2^{(8)}(m_\mu/m_e)$ by more than one independent method.

It is important to note that our classification of diagrams into groups (and subgroups) ensures that each subgroup is a *gauge-invariant* set. In fact, individual integrals are mostly not gauge-invariant and also infrared-divergent even when the UV-divergence is renormalized away. On the other hand, each gauge-invariant set is well-defined and relatively small due to strong cancellation among its constituents. This is dramatically demonstrated by $a_{IV(b)}$ and $a_{IV(c)}$ in (58), which are of order 1, whereas their constituents are 2 orders of magnitude larger as is seen from Table XI.

Empirically it is known that each mass-independent minimal gauge-invariant sets contributing to $g-2$ (namely diagrams containing no v-p loop or l-l loop) is of order 1 apart from a power of α/π. When v-p and/or l-l loops are inserted in such diagrams, they may acquire enhancements due to $\ln(m_\mu/m_e)$ factor, which is a con-

sequence of charge renormalization in case of v-p loop insertion and mass singularity present in the limit $m_e \to 0$ in the case of l-l loop. The size of *mass-dependent* terms contributing to $A_2^{(8)}(m_\mu/m_e)$ may be understood semi-quantitatively from this observation.

Let us now apply this argument to $M_{6LL,P2}^{(e,e)}$ in Table X, which is gauge-invariant and yet very large. Its size is inherited from the large sixth-order term M_{6LL}. The extraordinary size of M_{6LL} is due to the presence of $\ln(m_\mu/m_e)$ term with a large coefficient [6.38(8)] as was initially discovered by numerical integration [36]. It was noted then (unpublished) that it is numerically close to $2\pi^2/3$, later verified analytically [59], enabling us to write

$$M_{6LL} = \frac{2\pi^2}{3} \ln(m_\mu/m_e) + \cdots. \qquad (63)$$

Since M_{6LL} is UV-finite, the term $\ln m_\mu$ comes from the scale set by the largest physical mass of the system, m_μ. The $\ln m_e$ term arises from the integration of the momentum k of the l-l loop Λ_4 over the domain D_1 ($m_e < |k| < m_\mu$, $|p_i| \leq m_e$), where p_i, ($i = 1, 2, 3$) are the momenta of photons exchanged between the electron and the muon. Other domains such as D_3 (any k, $|p_i| > m_e$) does not contribute to $\ln m_e$.

What makes M_{6LL} really large, however, is the presence of the coefficient π^2 in (64). A physical interpretation for this fact was given by Elkhovsky [60] who pointed out that, in the subdomain D_2 ($m_e < |k| < m_\mu$, $|p_i| << m_e$, or more precisely $|p_i| \lesssim \alpha m_e$, $\alpha \simeq 1/137$) the muon is nearly at rest and the electron can be treated as a nonrelativistic particle in the field of the muon. One of the photons is responsible for the hyperfine spin-spin interaction, and the other two act essentially like a static Coulomb potential. It is the integration over the Coulomb photon momenta that gives a factor $i\pi$ each, contributing a factor $\pi^2(\sim 10)$ in (63).

Actually it is not easy to maintain the nonrelativistic behavior of the electron throughout the domain D_1 outside of D_2. This will result in the erosion of the enhancement factor π^2 in the domain $D_1 - D_2$, although the $\ln(m_\mu/m_e)$ behavior is still maintained. Together with nonlogarithmic contribution from other parts of momentum space, the net effect is to reduce the contribution of the leading term of (63), which is about 35, to about 21. This reduction may be expressed crudely by choosing the fudge factor ξ to be about 0.12 in

$$M_{6LL}^{(\text{approx})} = \frac{2\pi^2}{3} \ln(\xi m_\mu/m_e). \qquad (64)$$

Next consider the effect of the renormalized photon propagator:

$$D_R^{\mu,\nu}(q) = -i\frac{g_{\mu\nu}}{q^2} d_R(q^2/m_e^2, \alpha) + \cdots, \qquad (65)$$

where, to order α,

$$d_R(q^2/m_e^2, \alpha) = 1 + \frac{\alpha}{\pi}\left[\frac{1}{3}\ln(q^2/m_e^2) - \frac{5}{9} + \cdots\right]. \qquad (66)$$

When D_R is inserted in $g - 2$ diagrams, the scale for the momentum q is set by the muon mass. This means that the leading term of the integral containing a vacuum-polarization loop Π_2 such as $M_{6LL,P2}^{(e,e)}$ may be written as

$$M_{6LL,P2}^{(e,e)} \simeq 3KM_{6LL}^{(\text{approx})} + \text{terms linear in } \ln(m_\mu/m_e), \qquad (67)$$

where the factor three is the number of photon lines in which a vacuum-polarization loop can be inserted, and

$$K \equiv \frac{2}{3}\ln(m_\mu/m_e) - \frac{5}{9} \simeq 3, \qquad (68)$$

provided that q^2 is replaced by m_μ^2 in (66). The combination of these factors is responsible for the large size of the leading term of (67):

$$3 \times [(2/3)\ln(m_\mu/m_e) - 5/9] \times 20 \simeq 180, \qquad (69)$$

which is 1.5 times larger than the calculated value of $M_{6LL,P2}^{(e,e)}$ listed in Table X, pretty close for a crude approximation. If the argument given below Eq. (64) is applicable to the photon momenta, we would obtain $K \sim 1.7$ and (69) would become ~ 100. Both estimates would be acceptable as rough measure.

It is important to note that $M_{6LL,P2}^{(e,e)}$ is not only very large but also its value is known very precisely because it is obtained from the exactly known M_{6LL} by a well-understood vacuum-polarization insertion procedure. This means that the value of the term $A_2^{(8)}(m_\mu/m_e)$ is determined primarily by $a_{IV(a)}$ while its uncertainty comes mostly from $a_{IV(b)}$, $a_{IV(c)}$, and $a_{IV(d)}$. This is why the value of $A_2^{(8)}(m_\mu/m_e)$ did not change much even if $a_{IV(d)}$ suffered from a program error.

These arguments may also be applied in identifying the leading terms of the tenth-order contribution $A_2^{(10)}(m_\mu/m_e)$ [28].

ACKNOWLEDGMENTS

APPENDIX A: ELIMINATION OF ALGEBRAIC ERROR OF INTEGRALS

Most eighth-order integrals, including those of Group IV, are huge. A systematic approach is required to make sure that they are free from algebraic error and have forms suitable for numerical integration. To achieve this we adopted the following procedure:

(a) Carry out momentum integration of Feynman diagrams and convert them into integrals over Feynman parameters using algebraic manipulation program such as FORM [61]. This step is fully analytic. Conversion of all integrals of a gauge-invariant set is performed using a common *template* by permuting tensor indices of photon propagators.

(b) Integrals thus obtained are divergent in general. Since computers are not capable of handling divergence directly, both ultraviolet (UV) and infrared (IR) singularities must be removed from the integrand before integration is performed. In the subtractive on shell renormalization [62] of the nth order diagram M_n, the renormalization term involving a mth order vertex renormalization constant L_m is of the form $-L_m M_{n-m}$, where M_{n-m} is the $g-2$ term of order $n-m$. The subtraction procedure described in textbooks is not suitable for numerical integration, however, since it does not make the integrand of $M_n - L_m M_{n-m}$ finite throughout the domain of integration, as long as L_m is just a numerical constant.

The first step to achieve a pointwise cancellation is to express L_m as a parametric integral and combine it with the parametric integral of M_{n-m} using a generalization of Feynman's formula

$$\frac{1}{AB} = \int \frac{\delta(1 - z_1 - z_2)dz_1 dz_2}{(z_1 A + z_2 B)^2}, \qquad z_1, z_2 \geq 0. \tag{A1}$$

The domain of the combined integral $L_m \bigotimes M_{n-m}$ may then be chosen to be identical with that of M_n. Unfortunately, the integral is found to be intractable if we want to treat L_m as a whole. However, if it is split as

$$L_m = L_m^{(UV)} + L_m^{(IR)} + L_m^{(finite)}, \tag{A2}$$

where the UV-divergent part $L_m^{(UV)}$ is identified by the highest power of U, the IR-divergent part $L_m^{(IR)}$ by the highest power of V, $L_m^{(UV)} \bigotimes M_{n-m}$ is found to have a term-by-term correspondence with UV-divergent terms of the original (mother) integral M_n, and UV-divergences of M_n and $L_m^{(UV)} \bigotimes M_{n-m}$ cancel each other before (not after) integration is performed. [See (A6) for the definitions of U and V.] IR divergence can be handled in a similar way. This pointwise subtraction is crucial for the success of our renormalization program on a computer.

(c) In practice it is easier to start from the UV-divergent terms of the mother integral M_n, which can be readily identified by a power-counting at the singularity, and construct the subtraction term $L_m^{(UV)} \bigotimes M_{n-m}$ taking advantage of the term-by-term correspondence described above. This procedure, formalized as K-operation [see (A32) and (A33)] can be applied to all orders. Further advantage of the K-operation is that it can be readily implemented in the FORM program that generates the integrand of M_n. It is easy to confirm that the UV singularities of $L_m^{(UV)} \bigotimes M_{n-m}$ and M_n cancel out exactly by numerically evaluating the mother and daughter integrands at a sequence of points converging to the singular point.

(d) By construction the daughter integral factorizes *analytically* into a product of the *divergent part* of a renormalization constant and a magnetic moment of lower-order. Remaining parts of renormalization constants, such as $L_m^{(finite)}$, are summed over all diagrams afterwards. The result is a convergent integral of lower-order, which is easy to evaluate numerically. In other words, our renormalization proceeds in two steps. But, of course, it is identical with the standard on shell renormalization.

This procedure is designed to enable us to obtain extensive cross-checking at every step. To make this paper as self-contained as possible, let us describe them in some detail, although they can all be found in previous papers [57].

1. Construction of Feynman-parametric integral

Let G be a $2n$th order proper lepton vertex of QED, which describes the scattering of an incoming lepton of momentum $\not{p} - \not{q}/2$ by an external magnetic field into an outgoing lepton of momentum $\not{p} + \not{q}/2$, where both leptons are on the mass shell. G consists of $2n$ lepton propagators and n photon propagators of the form (in Feynman gauge)

$$\frac{\not{k}_i + \not{q}_i + m_i}{(k_i + q_i)^2 - m_i^2}, \qquad \frac{g_{\mu\nu}}{(k_i + q_i)^2 - m_i^2}, \qquad (A3)$$

besides factors describing the interaction, spinors, etc., Here k_i is a linear combination of the loop momenta flowing through the line i. q_i is a linear combination of external momenta. m_i is the mass associated with the line i, which is temporarily distinguished from each other for technical reasons. All these factors are combined to form a proper vertex part, which is integrated over n loop momenta.

The first step of momentum integration is to replace $\not{k}_i + \not{q}_i$ in the numerator of (A3) by an operator [63]

$$D_i^\mu \equiv \frac{1}{2} \int_{m_i^2}^\infty dm_i^2 \frac{\partial}{\partial q_{i\mu}} \qquad (A4)$$

for each lepton line i. Since D_i^μ does not depend on k_i explicitly, the numerator (turned into an operator now) can be pulled in front of momentum integration. The integrand then becomes just a product of denominators, which can be combined into one big function with the help of Feynman parameters $z_1, z_2, \ldots, z_N (N = 3n)$, assigned to respective propagators. Momentum integration can now be carried out exactly. D_i^μ can then be pulled back inside z integration. Omitting the factor $(\alpha/\pi)^n$ for simplicity the result can be expressed in the form

$$\Gamma_\nu^{(2n)} = \left(\frac{-1}{4}\right)^n (n-1)! \int \mathbf{F}_\nu \frac{(dz)_G}{U^2 V^n}, \qquad (A5)$$

where

$$(dz)_G = \delta\left(1 - \sum_{i=1}^N z_i\right) \prod_{i=1}^N dz_i,$$

$$V = \sum_{i=1}^N z_i(m_i^2 - q_i \cdot Q_i'), \qquad (A6)$$

$$Q_i'^\mu = -\frac{1}{U} \sum_{j=1}^N q_j^\mu z_j B_{ij}', \quad B_{ij}' = B_{ij} - \delta_{ij}\frac{U}{z_j}.$$

U and B_{ij} are homogeneous forms of degree n and $n-1$ in $z_1, \ldots, z_N$, respectively. (See [57] for explicit definitions.)

The operator $\mathbf{F}_\nu$ has the form

$$\mathbf{F}_\nu \propto \gamma^{\alpha_1}(\not{p}_1 + m_1)\gamma^{\alpha_2}(\not{p}_2 + m_2)\ldots\gamma_\nu\ldots\gamma^{\alpha_{(2n-1)}}$$
$$\times (\not{p}_{(2n)} + m_{(2n)})\gamma^{\alpha_{(2n)}}. \qquad (A7)$$

If G has closed lepton loops $\mathbf{F}_\nu$ contains some trace operations, too. The action of $\mathbf{F}^\nu$ on $1/V^n$ in (A5) produces terms of the form

$$\mathbf{F}^\nu \frac{1}{U^2 V^n} = \frac{F_0^\nu}{U^2 V^n} + \frac{F_1^\nu}{U^3 V^{n-1}} + \frac{F_2^\nu}{U^4 V^{n-2}} + \ldots, \qquad (A8)$$

where the subscript k of F_k^ν stands for the number of contractions. By contraction we mean picking a pair $\not{p}_i + m_i, \not{p}_j + m_j$ from $\mathbf{F}^\nu$, making the substitution

$$(\not{p}_i + m_i, \not{p}_j + m_j) \longrightarrow (\gamma^\mu, \gamma_\mu), \qquad (A9)$$

multiplying the result with $-\frac{1}{2}B_{ij}$, and summing them over all distinct pairs. Uncontracted D_i are replaced by Q_i'. For $k \geq 1$, F_k^ν includes an overall factor $(n-1)^{-1}\cdots(n-k)^{-1}$.

In our problem it is convenient to use, instead of the vector $Q_i'^\mu$ itself, a scalar function extracted from $Q_i'^\mu$. Suppose $p_\mu - q_\mu/2$ (external lepton momentum) enters the graph G at a point A, q_μ enters at a point C (which is the magnetic field vertex), and $p_\mu + q_\mu/2$ leaves at a point B. Then we may write

$$Q_i'^\mu = A_i^{(AC)}(p^\mu - q^\mu/2) + A_i^{(CB)}(p^\mu + q^\mu/2). \qquad (A10)$$

After a little manipulation we find, for example,

$$A_i^{(AB)} \equiv A_i^{(AC)} + A_i^{(CB)} = -\frac{1}{U}\sum_{j=1}^N \eta_{jP}(z_j B_{ji} - \delta_{ij}U),$$

$$P = P(AB). \qquad (A11)$$

associated with the path $P = P(AB)$ of the external momentum p, which is any self-nonintersecting path starting at A and ending at B, and $\eta_{jP} = (1, -1, 0)$ according to whether the line j lies (along, against, outside of) the path P. $A_i^{(AC)}$, $A_i^{(CB)}$, etc., are called "scalar currents" since they satisfy an analog of Kirchhoff's laws for electric currents when the diagram G is regarded as an electric network in which the Feynman parameter z_i plays the role of resistance [64]. B_{ij} satisfies Kirchhoff's laws, too. U and B_{ij} depend only on the topology of the graph G and not on whether the line is fermion or boson. They can be constructed easily from their definitions or by recursive relations starting from the one-loop case. We have written MAPLE and FORM programs to compute them algebraically for an arbitrary diagram. Once U and B_{ij} are known, $A_i \equiv A_i^{(AB)}$ can be constructed by (A11). For further details see [57].

The magnetic moment projection of $\Gamma_\nu^{(2n)}$ of the muon in *Version B* is given by

$$M_G^{(2n)B} = \lim_{q \to 0} Tr[P^\nu(p, q)\Gamma_\nu^{(2n)}], \qquad (A12)$$

where $(p + q/2)^2 = (p - q/2)^2 = m_\mu^2$, and

$$P^\nu(p,q) \equiv \frac{m_\mu}{16p^4q^2}\left(\not{p} - \frac{1}{2}\not{q} + m_\mu\right)[(\gamma^\nu\not{q} - \not{q}\gamma^\nu)p^2$$

$$- 3q^2 p^\nu]\left(\not{p} + \frac{1}{2}\not{q} + m_\mu\right). \tag{A13}$$

In the limit $q = 0$ the q^2 term can be dropped in the denominator V of (A5). Then V becomes a function of p^2 only and can be simplified to

$$V = \sum_{\text{all leptons}} z_i m_i^2 - G, \tag{A14}$$

where G is defined by

$$G = -\frac{1}{2}p^\nu\left(\frac{\partial V}{\partial p^\nu}\right)_{q^2=0, p^2=m_\mu^2}. \tag{A15}$$

G can be reduced further to the form

$$G = \sum_{\text{muon only}} z_i A_i m_\mu^2, \tag{A16}$$

by letting the external momentum p flows through consecutive muon lines only. This form is independent of how virtual photons are attached to muon lines. The information on photon attachment is contained in A_i. This provides a significant simplification in programming. Equation (A12) is the starting point of *Version B*.

In *Version A* the $g - 2$ term is projected out from the RHS of (14). In terms of Feynman parameters $z_1, z_2, \ldots z_N$, $(N = 3n - 1)$, introduced in the self-energy-like diagram G, the $2n$th order magnetic moment can be written as

$$M^{(2n)} = \left(\frac{-1}{4}\right)^n (n-1)! \int (dz)\left[\frac{\mathbf{E}+\mathbf{C}}{n-1}\frac{1}{U^2 V^{n-1}}\right.$$

$$\left. + (\mathbf{N}+\mathbf{Z})\frac{1}{U^2 V^n}\right], \tag{A17}$$

$\mathbf{E}, \mathbf{C}, \mathbf{N},$ and $\mathbf{Z}$ are pieces of the magnetic projection defined by

$$\mathbf{N} = \frac{1}{4}\text{Tr}[P_1^\nu p_\nu(2G\mathbf{F})], \qquad \mathbf{E} = \frac{1}{4}\text{Tr}[P_1^\nu \mathbf{E}_\nu],$$

$$\mathbf{C} = \frac{1}{4}\text{Tr}[P_2^{\mu\nu}\mathbf{C}_{\mu\nu}], \qquad \mathbf{Z} = \frac{1}{4}\text{Tr}[P_2^{\mu\nu}\mathbf{Z}_{\mu\nu}]. \tag{A18}$$

The factors P_1^ν and $P_2^{\mu\nu}$, derived from the magnetic projector P^ν of (A13) by averaging over the directions of q_μ subject to the constraint $q^\mu p_\mu = 0$, are of the form

$$P_1^\nu = \frac{1}{3}\gamma^\nu - \left(1 + \frac{4}{3}\frac{\not{p}}{m_\mu}\right)\frac{p^\nu}{m_\mu},$$

$$P_2^{\mu\nu} = \frac{1}{3}\left(\frac{\not{p}}{m_\mu} + 1\right)\left(g^{\mu\nu} - \gamma^\mu\gamma^\nu + \frac{p^\mu}{m_\mu}\gamma^\nu - \frac{p^\nu}{m_\mu}\gamma^\mu\right). \tag{A19}$$

The operator $\mathbf{F}$ is the numerator factor of the self-energy-like diagram G:

$$\mathbf{F} = \gamma^{\alpha_1}(\not{p}_1 + m_1)\gamma^{\alpha_2}(\not{p}_2 + m_2)\ldots\gamma^{\alpha_i}$$

$$\times (\not{p}_{(2n-1)} + m_{(2n-1)})\gamma^{\alpha_j}. \tag{A20}$$

Here i and j refer to the internal photon lines arriving at the $(2n - 1) - th$ and $2n$th vertices along the lepton line (which depend on the diagram G), $\mathbf{E}^\nu$ is defined by

$$\mathbf{E}^\nu \equiv \frac{\partial \mathbf{F}}{\partial p_\nu} = \sum_{\text{all leptons}} A_i \mathbf{F}_i^\nu, \tag{A21}$$

and $\mathbf{F}_i^\nu$ is obtained from $\mathbf{F}$ by the substitution in the ith line:

$$(\not{p}_i + m_i) \longrightarrow \gamma^\nu. \tag{A22}$$

$\mathbf{Z}_{\mu\nu}$ is defined by

$$\mathbf{Z}^{\mu\nu} = \sum_{j=1}^{2n-1} z_j \mathbf{Z}_j^{\mu\nu}, \tag{A23}$$

where $\mathbf{Z}_j^{\mu\nu}$ is obtained from $\mathbf{F}$ by the substitution

$$(\not{p}_j + m_j) \longrightarrow \frac{1}{2}[\gamma^\mu\gamma^\nu(\not{p}_j + m_j) - (\not{p}_j + m_j)\gamma^\nu\gamma^\mu]. \tag{A24}$$

$\mathbf{C}^{\mu\nu}$ is defined by

$$\mathbf{C}^{\mu\nu} = \sum_{i<j} C_{ij}\mathbf{F}_{ij}^{\mu\nu}, \tag{A25}$$

where

$$C_{ij} = \frac{1}{U^2}\sum_{k=1}^{2n-2}\sum_{l=k+1}^{2n-1} z_k z_l(B'_{ik}B'_{jl} - B'_{il}B'_{jk}), \tag{A26}$$

and $\mathbf{F}_{kl}^{\mu\nu}$ is obtained from $\mathbf{F}$ by the substitution

$$(\not{p}_k + m_k, \not{p}_l + m_l) \longrightarrow (\gamma^\mu, \gamma^\nu) \tag{A27}$$

in the kth and lth lepton lines. See (A6) for the definition of B'_{ik}.

Note that the potentially troublesome q^2 in the denominator of (A13) is absent in the formula (A18) so that the limit $q = 0$ can be taken without complication. As a consequence (A18) depends only on one external momentum p, and the only scalar current needed are A_i of the muon lines associated with p. When A_i are expressed in terms of B_{ij}'s, they have the same form for all diagrams irrespective of how virtual photons are attached to the muon line. This provides a useful simplification in programming.

We can now construct the integrand as follows:

(I) Express the integrand as a function of symbols B_{ij}, A_i, U, V for *Version B* and additional C_{ij} for *Version A*. This can be achieved by an algebraic program (such as FORM [61]) by which momentum integration is carried out exactly. All integrals are generated from a small number of *templates* by permutation of tensor indices of photon propagators.

(II) Quantities A_i, B_{ij}, C_{ij}, etc., introduced in (I) are just symbols. The next step is to turn them into explicit functions of Feynman parameters. This is facilitated by a common template which generates

B_{ij} and U for all diagrams sharing the same topological structure. Scalar currents A_i (and B_{ij}) must satisfy up to eight *junction laws* and four *loop laws* for each diagram. This provides very strong constraints on scalar currents and sets up a powerful defense against trivial programming error.

2. Construction of subtraction terms

Following the discussion (c) at the beginning of this Appendix let us now discuss more explicitly how to construct UV-divergence subtraction terms starting from the mother integral.

Suppose M_G is the magnetic moment contribution of a proper vertex part of $2n$th order defined by (A5) and (A12). Carrying out the D-operations in $\mathbf{F}_\nu$, one finds

$$M_G = -\left(\frac{-1}{4}\right)^n (n-1)! \int (dz)_G \left(\frac{F_0}{U^2 V^n} + \frac{F_1}{U^3 V^{n-1}}\right.$$
$$\left. + \frac{F_2}{U^4 V^{n-2}} + \cdots + \frac{F_{m_G}}{U^{m_G+2} V^{n-m_G}}\right), \quad \text{(A28)}$$

where m_G is the maximum number of contractions of D operators, which is equal to n for a vertex part. In (A28) the Feynman cutoff of photon propagators is not shown explicitly for simplicity.

Suppose M_G has an UV-divergence when all loop momenta of a subdiagram S consisting of N_S lines and n_S closed loops go to infinity. In the parametric formulation, this corresponds to the vanishing of the denominator U when all $z_i \in S$ vanish simultaneously. (Note that z_i is a sort of conjugate to k_i^2 in a Laplace transform.)

To find how an UV-divergence arises from S, consider the part of the integration domain where $z_i (\in S)$ satisfy $\sum_{i \in S} z_i \leq \epsilon$. In the limit $\epsilon \to 0$, one finds

$$V = \mathcal{O}(1), \qquad U = \mathcal{O}(\epsilon^{n_S}),$$
$$B_{ij} = \mathcal{O}(\epsilon^{n_S - 1}) \quad \text{if } i, j \in S,$$
$$B_{ij} = \mathcal{O}(\epsilon^{n_S}) \quad \text{otherwise.} \quad \text{(A29)}$$

Let m_S be the maximum number of contractions of D operators within S. Simple power-counting shows that the $(m+1)$st term of M_G, whose numerator has at most m_S factors of B_{ij}, $i, j \in S$, is divergent in the limit $\epsilon \to 0$ if and only if

$$N_S - 2n_S \leq \min[m, m_S], \quad \text{(A30)}$$

where $\min[m, m_S]$ means the lesser of m and m_S.

If S is a vertex part, we have $N_S = 3n_S$ and $m_S = n_S$. If S is an lepton self-energy part, we have $N_S = 3n_S - 1$ and $m_S = n_S - 1$. In both cases, (A30) is satisfied only for $\min[m, m_S] = m_S$, namely $m_S \leq m$. This means that the UV-divergence from S is restricted to the terms with m_S contractions within S in the last $m_G - m_S + 1$ terms of (A28).

Let us now introduce a $\mathbf{K}_S$ operation, which extracts the UV-divergent part (due to the subdiagram S) of the Feynman integral

$$M_G \equiv \int (dz)_G J_G \quad \text{(A31)}$$

in an analytically factorizable manner. This is achieved by the following steps:

(a) In the limit (A29) keep only terms with the lowest power of ϵ in U, B_{ij}, A_i, V. [U then factorizes into a product of U_S and U_R, where U_S, U_R are U-functions defined on S, R, respectively, and $R \equiv G/S$ is obtained from G by shrinking S to a point. Similarly for B_{ij}. V is reduced to V_R. Factorization of A_i is more subtle since it has U in its denominator. The recipe here is to keep only those terms of A_i whose numerator is a linear combination of B_{ij} with $i, j \in S$. This is necessary for analytic factorization to work.]

(b) Replace V_R obtained in (a) by $V_R + V_S$, where V_S is a V function defined on S. [Since $V_S = \mathcal{O}(\epsilon)$ whereas $V_R = \mathcal{O}(1)$, this does not affect the leading singularity of the integrand in the $\epsilon \to 0$ limit.

(c) Rewrite J_G in terms of the redefined parametric functions, drop all terms except those with m_S contractions within S, and call the result $\mathbf{K}_S M_G$.

Since we deal in practice with logarithmic divergence only, the steps (a), (b), and (c) are sufficient to ensure that $(1 - \mathbf{K}_S)M_G$ is convergent for $\epsilon \to 0$. The inclusion of V_S in (b) serves two purposes. One is to avoid spurious singularity which V_R alone might develop in other parts of the integration domain, and the other is to enables us to decompose $\mathbf{K}_S M_G$ (assuming S is a vertex part) into a product of lower-order factors *analytically* as

$$\mathbf{K}_S M_G = \hat{L}_S M_{G/S}, \quad \text{(A32)}$$

where $\hat{L}_S$ is the UV-divergent part of the renormalization constant L_S.

If S is a lepton self-energy part inserted between consecutive lepton lines i and j of G, we obtain a slightly more complicated result

$$\mathbf{K}_S M_G = \delta\hat{m}_S M_{G/S(i*)} + \hat{B}_S M_{G/S(i')} \quad \text{(A33)}$$

Here $\hat{B}_S$ and $\delta\hat{m}_S$ are UV-divergent parts of renormalization constants B_S and δm_S. Since $\hat{L}_S, M_{G/S}$, etc., are quantities of lower-orders, they are already known or can be easily constructed from scratch.

Note that Eqs. (A32) and (A33) are quite nontrivial since the LHS are defined over the entire n-dimensional surface while the RHS are products of integrals over lower-dimensional spaces. Identification of the second term on the RHS of (A33) requires further work involving an integration-by part. (See [57] for details.)

An IR divergence, which is caused by vanishing virtual photon momentum, arises from the part of integration domain R where z_i's assigned to the photon takes the

largest possible value under the constraint $\sum z_i = 1$. All other z_i's are pushed to zero in the IR limit. Furthermore, the IR-singularity, in order that it actually becomes divergent, must be enhanced by vanishing denominators of muon propagators adjacent to the infrared photon. In parametric language this corresponds to the vanishing of V as $V \sim \delta^2$ for $\delta \to 0$ in the integration domain characterized by

$$z_i = \begin{cases} O(\delta) & \text{if } i \text{ is a muon line in } R \\ O(1) & \text{if } i \text{ is a photon line in } R \\ O(\delta^2) & \text{if } i \text{ is in } G/R. \end{cases}$$

Starting from this one can obtain a power-counting rule which enables us to identify IR-divergent terms in a way analogous to that of UV-divergence. The criteria to be satisfied by the IR subtraction operator $\mathbf{I}_R$ are

  (i) it subtracts the IR-divergent part of the mother integrand completely,

  (ii) it factorizes analytically into a product of IR-divergent part of renormalization constant and magnetic moment of lower-orders.

The difference with $\mathbf{K}_S$ operation is that we must now look for largest negative powers of V instead of U in (A28). See [57] for details.

3. Diagrams containing a second-order lepton self-energy part

When an integrand containing a second-order electron self-energy part S is expressed as a function of scalar currents, all of its terms contribute to the UV-divergence. This means that the integrand of the self-energy subtraction term, *when expressed in terms of its own scalar currents*, has a form identical with that of a mother integrand. Their difference comes solely from different structures of scalar currents for mother and daughter integrals. This provides the simplest example of (A33).

To demonstrate it explicitly let us go back to the vertex (A5) and rewrite $\mathbf{F}_\nu$ of (A7) to exhibit the self-energy part S explicitly:

$$\begin{aligned}
\mathbf{F}_\nu = {} & \gamma^{\alpha_1}(\not{p}_1 + m_1)\gamma^{\alpha_2}(\not{p}_2 + m_2)\ldots\gamma^{\alpha_{(i-1)}} \\
& \times (\not{p}_{(i-1)} + m_{(i-1)})\gamma^\beta(\not{p}_{(i)} + m_{(i)})\gamma_\beta \\
& \times (\not{p}_{(i+1)} + m_{(i+1)})\ldots\gamma^{\alpha_{(2n-1)}}(\not{p}_{(2n)} + m_{(2n)})\gamma^{\alpha_2 n},
\end{aligned}$$
(A34)

where $\gamma^\beta(\not{p}_{(i)} + m_{(i)})\gamma_\beta$ comes from the second-order lepton self-energy part S. (γ_ν is not shown explicitly.) Carrying out the contraction of γ^β and γ_β this factor can be written as $2m_{(i)} - 2(\not{p}_{(i)} - m_{(i)})$. This leads naturally

to the decomposition

$$\mathbf{F}_\nu = \mathbf{F}_\nu^{(1)} + \mathbf{F}_\nu^{(2)}, \tag{A35}$$

where $\mathbf{F}_\nu^{(1)}$ and $\mathbf{F}_\nu^{(2)}$ are obtained by replacing $\gamma^\beta(\not{p}_{(i)} + m_{(i)})\gamma_\beta$ of (A34) by $2m_{(i)}$ and $-2(\not{p}_{(i)} - m_{(i)})$, respectively.

As is easily seen the $\mathbf{F}_\nu^{(1)}$ part of the integral $\mathbf{K}_S M_G$ factorizes exactly into a product of the self-mass δm_2 and the term $M_{G/S(i^*)}$, which is obtained from M_G by shrinking the lepton self-energy diagram S to a point:

$$\delta m_2 M_{G/S(i^*)}. \tag{A36}$$

In the same limit the $\mathbf{F}_\nu^{(2)}$ part of the integral $\mathbf{K}_S M_G$ factorizes exactly into a product of $\hat{B}_2$ [the UV-divergent part of B_2 (see [57])] and the term $M_{G/S(i')}$, which is obtained by inserting the factor $-(\not{p}_{(i)} - m_{(i)})$ in $M_{G/S(i^*)}$:

$$\hat{B}_2 M_{G/S(i')}. \tag{A37}$$

Note that in the $\mathbf{K}_S M_G$ operation leading to (A37) the contraction of $D_{(i)}$ with other D's in G are dropped.

Finally, using an identity

$$\int (dz)_G \frac{F_0}{U^2 V^{N-2n}} = -\int (dz)_G z_j \frac{\partial}{\partial z_j}\left(\frac{F_0}{U^2 V^{N-2n}}\right), \tag{A38}$$

which is a particular case of Eq. (A.7) of Nakanishi's Appendix [65], one can transform $M_{G/S(i')}$ into an amplitude $M_{G/[S,i+1]}$, which is obtained by removing the self-energy part S and the adjacent lepton line $i + 1$ from G. (This is identical with a vertex of lower-order obtained directly by Feynman-Dyson rules.)

4. An Illustration: Two-Step Renormalization of Fourth-Order Magnetic Moment

The formulation described above is illustrated here by applying it to the fourth-order magnetic moment M_4 in *Version A*, which consists of two parts M_{4a} and M_{4b}. Equation (A17) applied to the diagram $G = [1, 2, 3, 4, 5]$ of Fig. 8(d) leads to

$$M_{4a} = \frac{1}{16}\int (dz)\left(\frac{E_0 + C_0}{U^2 V} + \frac{N_0 + Z_0}{U^2 V^2} + \frac{N_1 + Z_1}{U^3 V}\right), \tag{A39}$$

where , for simplicity, Feynman cutoff of photon lines is not shown explicitly [37,57]. Numerator functions are expressed in terms of scalar currents A_i and B_{ij}:

$$\begin{aligned}
& E_0 = 8(2A_1 A_2 A_3 - A_1 A_2 - A_1 A_3 - A_2 A_3), \quad C_0 = -24z_4 z_5/U, \quad N_0 = G[E_0 - 8(2A_2 - 1)], \\
& Z_0 = 8z_1(-A_1 + A_2 + A_3 + A_1 A_2 + A_1 A_3 - A_2 A_3) + 8z_2(1 - A_1 A_2 + A_1 A_3 - A_2 A_3 + 2A_1 A_2 A_3) \\
& \qquad + 8z_3(A_1 + A_2 - A_3 - A_1 A_2 + A_1 A_3 + A_2 A_3), \quad N_1 = 8G[B_{12}(2 - A_3) + B_{13}(2 - 4A_2) + B_{23}(2 - A_1)], \\
& Z_1 = -8z_1[B_{12}(1 - A_3) + B_{13} + B_{23}A_1] + 8z_2[B_{12}(1 - A_3) - 4B_{13}A_2 + B_{23}(1 - A_1)] \\
& \qquad - 8z_3[B_{12}A_3 + B_{13} + B_{23}(1 - A_1)],
\end{aligned} \tag{A40}$$

in addition to $z_1, z_2, z_3,$ and G, and

$$B_{11} = z_{235}, \quad B_{12} = z_{35}, \quad B_{13} = -z_2, \quad B_{23} = z_{14}, \quad B_{22} = z_{1345}, \quad B_{33} = z_{124},$$
$$U = z_2 B_{12} + z_{14} B_{11}, \quad A_i = 1 - (z_1 B_{1i} + z_2 B_{2i} + z_3 B_{3i})/U, \quad i = 1, 2, 3, \quad G = z_1 A_1 + z_2 A_2 + z_3 A_3, \tag{A41}$$
$$V = z_{123} - G, \quad (dz) = \delta(1 - z_{12345})dz_1 dz_2 dz_3 dz_4 dz_5, \quad z_{235} \equiv z_2 + z_3 + z_5.$$

The integral for M_{4b} of Fig. 8(e) has the same form as (A39) but has different definitions of functions [37,57]:

$$E_0 = 8A_1[4(A_2 - A_1) - A_1 A_2], \quad C_0 = -8A_2, \quad N_0 = -8G[4(1 - A_1 + A_1^2) + A_2(1 - 4A_1 + A_1^2)].$$
$$Z_0 = 8z_{13}[4A_1 - A_2(1 + A_1^2)] + 8z_2 A_2(1 + A_1^2), \quad N_1 = 8G[8(B_{11} - B_{12}) + 3A_1 B_{12}], \quad Z_1 = 24(z_{13} - z_2)A_1 B_{12}, \tag{A42}$$

where

$$B_{11} = z_{24}, \qquad B_{12} = z_4, \qquad B_{22} = z_{1345},$$
$$U = z_{135}B_{11} + z_2 B_{12}, \qquad A_1 = z_5 B_{11}/U,$$
$$A_2 = z_5 B_{12}/U, \qquad G = z_{13}A_1 + z_2 A_2, \tag{A43}$$
$$V = z_{123} - G.$$

The standard on shell renormalized amplitudes a_{4a} and a_{4b} are defined by

$$a_{4a} = M_{4a} - 2L_2 M_2 \tag{A44}$$

and

$$a_{4b} = M_{4b} - \delta m_2 M_{2^*} - B_2 M_2. \tag{A45}$$

We carry out the renormalization in two steps, expressing all quantities as parametric integrals. For instance, the magnetic moment M_2 is written in the form (putting $m_4 = 0$ in V)

$$M_2 = -\frac{1}{4}\int (dz)\frac{N_0 + Z_0}{U^2 V}, \qquad N_0 + Z_0 = 4G(A_1 - 1), \tag{A46}$$

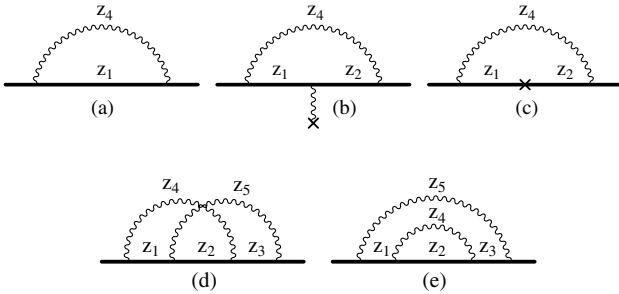(a)   (b)   (c)

(d)   (e)

FIG. 8.   Assignment of Feynman parameters $z_1 \ldots z_5$ is shown for (a) second-order self-energy diagram, (b) second-order vertex diagram, (c) second-order self-energy diagram in which a 2-point vertex is inserted, (d) fourth-order diagram M_{4a}, (e) fourth-order diagrams M_{4b}. Horizontal lines [except in (b)] are lepton lines in the presence of the magnetic field. Each of diagrams (d) and (e) represents the sum of three fourth-order vertex diagrams.

where

$$B_{11} = 1, \qquad U = z_{14}B_{11}, \qquad A_1 = z_4/U,$$
$$G = z_1 A_1, \qquad V = z_1 + m_4^2 z_4 - G, \tag{A47}$$
$$(dz) = \delta(1 - z_{14})dz_1 dz_4, \qquad z_{14} \equiv z_1 + z_4.$$

Following the general discussion the parametric integrals of B_2 and δm_2 are split into UV-divergent parts $\hat{B}_2$ and $\delta \hat{m}_2$ and UV-finite part $\tilde{B}_2$ and $\delta \tilde{m}_2$:

$$B_2 = \hat{B}_2 + \tilde{B}_2, \qquad \delta m_2 = \delta \hat{m}_2 + \delta \tilde{m}_2, \tag{A48}$$

where

$$\hat{B}_2 = \frac{1}{4}\int (dz)\int_{\lambda^2}^{\Lambda^2} z_4 dm_4^2 \frac{E_0}{U^2 V}, \qquad E_0 = -2A_1,$$
$$\tilde{B}_2 = \frac{1}{4}\int (dz)\frac{N_0}{U^2 V}, \qquad N_0 = 2G(4 - 2A_1),$$
$$\delta \hat{m}_2 = \frac{1}{4}\int (dz)\int_{\lambda^2}^{\Lambda^2} z_4 dm_4^2 \frac{F_0}{U^2 V}, \tag{A49}$$
$$F_0 = 2(2 - A_1), \qquad \delta \tilde{m}_2 = 0.$$

$A_1, U, V, (dz)$ are the same as in (A40) and Λ and λ are UV and IR cutoffs for the virtual photon mass m_4. The UV cutoff is removed from $\tilde{B}_2$ since it is not UV-divergent.

Similarly, we split the vertex renormalization constant L_2 for Fig. 8(b) as $\hat{L}_2 + \tilde{L}_2$, where

$$\hat{L}_2 = -\frac{1}{4}\int (dz)\int_{\lambda^2}^{\Lambda^2} z_4 dm_4^2 \frac{F_1}{U^3 V}, \quad F_1 = -2B_{11},$$
$$\tilde{L}_2 = -\frac{1}{4}\int (dz)\frac{F_0}{U^2 V}, \quad F_0 = -2(1 - 4A_1 + A_1^2), \tag{A50}$$

where

$$B_{11} = 1, \qquad U = z_{124}B_{11}, \qquad A_1 = z_4/U,$$
$$G = z_{12}A_1, \qquad V = z_{12} + m_4^2 z_4 - G, \tag{A51}$$
$$(dz) = \delta(1 - z_{124})dz_1 dz_2 dz_4.$$

Finally we need M_{2^*} (magnetic moment contribution of the diagrams in Fig. 8(c)):

$$M_{2^*} = \frac{2}{4} \int (dz) \left(\frac{N_0^* + Z_0^*}{U^2 V^2} + \frac{N_1^*}{U^3 V} + \frac{E_0^*}{U^2 V} \right),$$

$$N_0^* + Z_0^* = -8GA_1(A_1 - 1), \qquad N_1^* = 16GB_{11}, \qquad (A52)$$

$$E_0^* = -8A_1^2,$$

where functions are the same as in (A51).

a. Two-step renormalization of M_{4a}.

The first step is to rewrite (A44) as

$$a_{4a} = \Delta M_{4a} + [(\mathbf{K}_{12} + \mathbf{K}_{23})M_{4a} - 2L_2 M_2]. \qquad (A53)$$

$\mathbf{K}_{12}$ is an UV-divergence extraction operator for the vertex subdiagram $S \equiv [1, 2, 4]$. The integral

$$\Delta M_{4a} = (1 - \mathbf{K}_{12} - \mathbf{K}_{23})M_{4a} \qquad (A54)$$

is UV-finite by construction. $\mathbf{K}_{12}M_{4a}$ can be written as

$$\mathbf{K}_{12}M_{4a} = \frac{1}{16} \int (dz) \int_{\lambda^2}^{\Lambda^2} z_4 dm_4^2 \frac{N_1' + Z_1'}{U'^3 V'^2}, \qquad (A55)$$

where the Feynman cutoff of photon mass m_4 is shown explicitly and

$$B_{12} = z_{35}, \quad U' = z_{124}B_{12}, \quad A_3' = z_5/z_{35},$$

$$A_1' = z_4/z_{124}, \quad G' = z_3 A_3',$$

$$V' = z_{123} + m_4^2 z_4 - G' - z_{12} A_1',$$

$$N_1' + Z_1' = 8G'B_{12}(1 - A_3').$$

$\mathbf{K}_{23}M_{4a}$ for the vertex diagram [2,3,5] can be constructed in a similar way.

To show that (A55) can be factorized and reduced to the RHS of (A32), let $T \equiv [3, 5]$ be the reduced diagram obtained from G by shrinking S to a point. Let us define $z_S \equiv z_{124}, z_T \equiv z_{35}$, and introduce Feynman parameters x_i and y_j for the sets S and T in such a way that

$$x_1 = z_1/z_S, \qquad x_2 = z_2/z_S, \qquad x_4 = z_4/z_S,$$

$$y_3 = z_3/z_T, \qquad y_5 = z_5/z_T.$$

Then, after few steps of manipulation, which amounts to the substitution

$$B_{12} \to B_{12}^T(=1), \quad A_3' \to A_3^T(=y_3/y_{35}), \quad G' \to y_3 A_3^T,$$

$$U' \to U_S U_T, \qquad V' \to z_S V_S + z_T V_T,$$

$$N_1' + Z_1' \to 8y_3 A_3^T(1 - A_3^T),$$

with

$$A_1^S = x_4/x_{124}, \qquad U_S = z_S, \qquad U_T = z_T,$$

$$V_S = x_{12} + m_4^2 x_4 - G_S, \qquad V_T = y_3 - G_T,$$

$$G_S = x_{12} A_1^S, \qquad G_T = y_3 A_3^T,$$

we can rewrite (A55) as

$$\mathbf{K}_{12}M_{4a} = \frac{1}{16} \int (dx) \int (dy) \int (d\tilde{z})$$

$$\times \int_{\lambda^2}^{\Lambda^2} x_4 dm_4^2 \frac{8y_3 A_3^T(1 - A_3^T)}{(z_S V_S + z_T V_T)^2}, \qquad (A56)$$

where $(d\tilde{z}) \equiv \delta(1 - z_S - z_T)dz_S dz_T$. Note that U' in (A55) factorized as $U_S U_T$, and they canceled out completely against z_S and z_T in the numerator. Since z_S and z_T now appear linearly in the denominator only, the z-integration can be carried out explicitly using Eq. (A1) which reduces the integral (A56) to a product of $\hat{L}_2$ and M_2:

$$\mathbf{K}_{12}M_{4a} = \hat{L}_2 M_2. \qquad (A57)$$

This is a particular case of (A32). Similarly for $\mathbf{K}_{23}M_{4a}$. Note that $\mathbf{K}$-operation extracts only the UV-divergent part $\hat{L}_2$ of L_2. This exact factorization of (A57) is generalizable to all orders, which is crucial for carrying the two-step renormalization scheme over to higher orders.

From (A44), (A50), and (A57) we obtain

$$a_{4a} = \Delta M_{4a} - 2\tilde{L}_2 M_2, \qquad (A58)$$

where both terms on the right-hand side are UV-finite. ($\tilde{L}_2$ is IR-divergent.)

b. Two-step renormalization of M_{4b}.

We begin by rewriting (A45) as

$$a_{4b} = \Delta' M_{4b} + (\mathbf{K}_2 M_{4b} - \delta m_2 M_{2^*} - B_2 M_2). \qquad (A59)$$

$\mathbf{K}_2$ isolates the UV-divergence of M_{4b} arising from the self-energy subdiagram $S \equiv [2, 4]$. By construction the integral

$$\Delta' M_{4b} = (1 - \mathbf{K}_2)M_{4b} \qquad (A60)$$

is UV-finite. Following the rule given in Appendix A2, $\mathbf{K}_2 M_{4b}$ is obtained by dropping terms in Z_0 and Z_1 of (A42) that contains z_2 explicitly (z_2 and z_4 hidden within A_i and B_{ij} must be kept to the leading order in the $\mathbf{K}_2$ limit.) Noting that $A_2 \to A_1' A_2'$ in the $\mathbf{K}_2$-limit we find from (A42)

$$E_0' = 8A_1'^2[4(A_2' - 1) - A_1'A_2'], \quad C_0' = -8A_1'A_2',$$

$$N_0' = -8G'[4(1 - A_1' + A_1'^2) + A_1'A_2'(1 - 4A_1' + A_1'^2)].$$

$$Z_0' = 8z_{13}A_1'[4 - A_2'(1 + A_1'^2)],$$

$$N_1' = 8G'[8(B_{11}' - B_{12}') + 3A_1'B_{12}'], \qquad (A61)$$

$$Z_1' = 24z_{13}A_1'B_{12}',$$

where

$$A_1' = z_5/z_{135}, \qquad A_2' = z_4/z_{24}, \qquad G' = z_{13}A_1',$$

Including the regulator mass m_4 of photon four explicitly, we can express $\mathbf{K}_2 M_{4b}$ as

$$\mathbf{K}_2 M_{4b} = \frac{1}{16} \int (dz) z_4 \int_{\lambda^2}^{\Lambda^2} dm_4^2 \left[\frac{E_0' + C_0'}{U'^2 V'^2} + \frac{2(N_0' + Z_0')}{U'^2 V'^3} \right. $$
$$\left. + \frac{N_1' + Z_1'}{U'^3 V'^2} \right]. \tag{A62}$$

In the $\mathbf{K}_2$-limit U' and V' decompose as

$$U' \rightarrow U_S' U_T', \qquad V' \rightarrow z_S V_S'' + z_T V_T'', \tag{A63}$$

where $U_S' = z_S = z_{24}$, $U_T' = z_T = z_{135}$, and V_S'' and V_T'' are

V functions for the subdiagrams $S \equiv [2, 4]$ and $T \equiv [1, 3, 5]$ to be made explicit in the following.

Let us introduce Feynman parameters x_i and y_i for the subdiagrams S and T as follows:

$$x_2 = z_2/z_S, \qquad x_4 = z_4/z_S,$$
$$y_1 = z_1/z_T, \qquad y_3 = z_3/z_T, \qquad y_5 = z_5/z_T,$$

and rewrite (A62) in terms of

$$
\begin{array}{llllll}
B_{11}' = x_{24} z_S, & B_{12}' = x_4 z_S, & A_1' = y_5/y_{135}, & A_2' = x_4/x_{24}, & G_S = x_2 A_2', & G_T = y_{13} A_1', \\
U_S' = z_S U_S'', & U_S'' = x_{24}, & U_T' = z_T U_T'', & U_T'' = y_{135}, & & \\
V' = z_S V_S'' + z_T V_T'', & V_S'' = x_2 + m_4^2 x_4 - G_S, & V_T'' = y_{13} - G_T, & & & \\
(dx) = \delta(1 - x_{24}) dx_2 dx_4, & (dy) = \delta(1 - y_{135}) dy_1 dy_3 dy_5. & & & &
\end{array}
\tag{A64}
$$

Then, dropping superscripts $'$ and $''$ for simplicity, we can reexpress (A62) as

$$\mathbf{K}_2 M_{4b} = \frac{1}{16} \int (dx) \int (dy) \int (d\bar{z}) \int_{\lambda^2}^{\Lambda^2} x_4 dm_4^2 \left\{ \frac{z_S^{2-2} z_T^{2-2}}{U_S^2 U_T^2} \frac{8A_1^2[4(A_2 - 1) - A_1 A_2)] - 8A_1 A_2}{(z_S V_S + z_T V_T)^2} + \frac{z_S^{2-2} z_T^{3-2}}{U_S^2 U_T^2} \right.$$
$$\times \frac{-16 G_T[4(1 - A_1 + A_1^2) + A_1 A_2 (1 - 4A_1 + A_1^2) - (4 - A_2(1 + A_1^2))]}{(z_S V_S + z_T V_T)^3} + \frac{z_S^{3-3} z_T^{3-3}}{U_S^3 U_T^3}$$
$$\left. \times \frac{8 G_T[8(B_{11} - B_{12}) + 3A_1 B_{12} + 3B_{12}]}{(z_S V_S + z_T V_T)^2} \right\}, \tag{A65}$$

where

$$(d\bar{z}) = \delta(1 - z_S - z_T) dz_S dz_T.$$

Now the $\bar{z}$ integration can be carried out exactly using (A1). The result is

$$\mathbf{K}_2 M_{4b} = \frac{1}{16} \int (dx) \int (dy) \int_{\lambda^2}^{\Lambda^2} x_4 dm_4^2 \left\{ \frac{8A_1^2[4(A_2 - 1) - A_1 A_2] - 8A_1 A_2}{U_S^2 V_S U_T^2 V_T} \right.$$
$$+ \frac{-8 G_T[4(1 - A_1 + A_1^2) + A_1 A_2 (1 - 4A_1 + A_1^2) - (4 - A_2(1 + A_1^2))]}{U_S^2 V_S U_T^2 V_T^2}$$
$$\left. + \frac{8 G_T B_{11}[8(1 - A_2) + 3A_1 A_2 + 3A_2]}{U_S^3 V_S U_T^3 V_T} \right\}, \tag{A66}$$

where $B_{12}/B_{11} = A_2$ is used. Decomposing the numerator of each term into terms proportional to $(2 - A_2)$ and A_2 following (A35), we can rewrite (A66) as

$$\mathbf{K}_2 M_{4b} = \frac{1}{16} \int (dx) \int_{\lambda^2}^{\Lambda^2} x_4 dm_4^2 \frac{2 - A_2}{U_S^2 V_S} \int (dy) \left[\frac{-16 A_1^2}{U_T^2 V_T} + \frac{-16 G_T(-A_1 + A_1^2)}{U_T^2 V_T^2} + \frac{32 G_T B_{11}}{U_T^3 V_T} \right] + \frac{1}{16} \int (dx)$$
$$\times \int_{\lambda^2}^{\Lambda^2} x_4 dm_4^2 \frac{A_2}{U_S^2 V_S} \int (dy) \left[\frac{8A_1^2(2 - A_1) - 8A_1}{U_T^2 V_T} + \frac{-8 G_T(1 - A_1 - A_1^2 + A_1^3)}{U_T^2 V_T^2} + \frac{2 G_T B_{11}(-4 + 12 A_1)}{U_T^3 V_T} \right]. \tag{A67}$$

Note that both terms are now just products of x-integral and y-integral. Comparing them with (A49) and (A52), it is easy to see that the first term is $\delta m_2 M_{2*}$, which corresponds to the first term of (A33). The x-integral of the second term is proportional to $\hat{B}_2$. Thus the remaining task is to identify the y-integral with M_2 in (A49). The first step of demonstration is to transform M_2 by an integration-by-part. Dropping the suffix T for simplicity, we obtain

$$M_2 = \int (dy) \frac{y_1 A_1(1 - A_1)}{U^2 V}$$
$$= -\int (dy) y_1 \frac{\partial}{\partial y_1} \left[\frac{y_1 A_1(1 - A_1)}{U^2 V} \right]$$
$$= -\int (dy) y_1 \left[\frac{A_1(1 - A_1)}{U^2 V} + \frac{y_1 B_{11}(-3A_1 + 4A_1^2)}{U^3 V} \right.$$
$$\left. - \frac{y_1 A_1(1 - A_1)(1 - A_1^2)}{U^2 V^2} \right], \tag{A68}$$

where we have used

$$B_{11} = 1, \qquad U = y_{14}B_{11}, \qquad A_1 = \frac{y_4 B_{11}}{U},$$

$$\frac{\partial U}{\partial y_1} = B_{11}, \qquad \frac{\partial A_1}{\partial y_1} = -\frac{A_1 B_{11}}{U}, \qquad \frac{\partial V}{\partial y_1} = 1 - A_1^2.$$

Noting that $y_1 B_{11}/U = 1 - A_1$, (A68) can be reduced to

$$M_2 = \int (dy) y_1 \left[\frac{2A_1(1 - A_1)(1 - 2A_1)}{U^2 V} + \frac{y_1 A_1(1 - A_1)(1 - A_1^2)}{U^2 V^2} \right]. \qquad (A69)$$

It is now easy to see that (A69) is proportional to the second y-integral of (A67). One has only to note that $(dy)y_1 = \delta(1 - y_1 - y_4)y_1 dy_1 dy_4$ in (A69) is equivalent to $(dy) = \delta(1 - y_1 - y_3 - y_5) dy_1 dy_3 dy_5$ in (A67) since its integrand depends on the sum $y_1 + y_3$ only. Equation (A68) is a special case of (A38).

Making use of formulas for δm_2, $\hat{B}_2$, and M_{2*} in (A49) and (A52), we thus obtain

$$\mathbf{K}_2 M_{4b} = \delta m_2 M_{2*} + \hat{B}_2 M_2, \qquad (A70)$$

which is a particular case of (A33).

Using (A59) and (A60) a_{4b} in (A45) can be rewritten as

$$a_{4b} = \Delta' M_{4b} - \tilde{B}_2 M_2. \qquad (A71)$$

Both terms on the right-hand side are UV-finite although $\Delta' M_{4b}$ is IR-divergent.

c. Separation of IR divergence in $\Delta' M_{4b}$.

The sum $a_{4a} + a_{4b}$ is UV- and IR-finite. However, for numerical evaluation it is necessary to remove IR-divergent terms from the integral $\Delta' M_{4b}$. This is where Step 2 comes in. A general procedure for isolating the IR-divergent terms is given in [57]. Power-counting shows that, of three vertex diagrams contributing to $\Delta' M_{4b}$, IR divergence arises only from the vertex in which the magnetic field acts on the muon line denoted z_2 in Fig. 8(e). More specifically, it arises from the domain

$$z_5 = 1 - \mathcal{O}(\delta), \qquad z_1, z_3 = \mathcal{O}(\delta), \qquad z_2, z_4 = \mathcal{O}(\delta^2), \qquad (A72)$$

where $\delta \sim \lambda$ and λ is the photon mass. In this domain one may define an IR-extracting operator $\mathbf{I}_T$ by

$$U \to U_S U_T, \qquad V \to V_S + V_T, \qquad V_S = z_2(1 - A_2),$$
$$V_T = z_{13}(1 - A_1) + z_5 m_5^2. \qquad A_1 = z_5/z_{135},$$
$$A_2 = z_4/z_{24}, \qquad U_S = z_{24}, \qquad U_T = z_{135}. \qquad (A73)$$

This definition is actually identical with that of the $\mathbf{K}_2$-limit (A62) except that the substitution $A_2 \to A_1' A_2'$ [see above Eq. (A61)] is replaced by $A_2 \to A_2' (\Rightarrow A_2)$.

The separation of IR-divergent term of $\Delta' M_{4b}$ may be written as

$$\Delta' M_{4b} = \Delta M_{4b} + \mathbf{I}_T \Delta' M_{4b},$$

where

$$\Delta M_{4b} = (1 - \mathbf{I}_T) \Delta' M_{4b}. \qquad (A74)$$

The definition (A73), although it picks up the IR-singularity correctly, is actually not complete until an appropriate numerator function is chosen. We chose to define the IR separation operator $\mathbf{I}_T$, $T \equiv [1, 3, 5]$, by

$$\mathbf{I}_T \Delta' M_{4b} = \frac{1}{16} \int (dz) \frac{F_T F_S}{U^2 V^2}, \qquad (A75)$$

where

$$F_T = -2(1 - 4A_1 + A_1^2), \qquad F_S = -4z_2 A_2(1 - A_2). \qquad (A76)$$

F_T is chosen to coincide with F_0 of (A50) and F_S corresponds to $N_0 + Z_0$ of (A46). After taking steps analogous to (A63) and (A64), this choice leads to an exact factorization of the integral (A75) as a product of known second-order integrals

$$\mathbf{I}_T \Delta' M_{4b} = \tilde{L}_2 M_2. \qquad (A77)$$

Note that a particular choice of numerator is not crucial as far as it deals with the IR divergence correctly since what is subtracted must be put back in the end.

Summing up all terms we obtain

$$a_4 = a_{4a} + a_{4b} = \Delta M_{4a} + \Delta M_{4b} - \Delta B_2 M_2 \qquad (A78)$$

where $\Delta B_2 \equiv \tilde{L}_2 + \tilde{B}_2 (= 3/4)$ and $M_2 = 1/2$. Numerical evaluation of ΔM_{4a} and ΔM_{4b} gives

$$\Delta M_{4a} = 0.218\,342(17), \qquad \Delta M_{4b} = -0.187\,501(14),$$
$$a_4 = -0.344\,158(22), \qquad (149)$$

which is an update of the old evaluation [57]. It is in good agreement with the analytical value $-0.344\,166\cdots$.

We described the fourth-order case in full detail because it will serve as a good prototype for higher-order cases. To begin with integrals such as (A39) with integrands (A40) and (A42) are obtained by a simple algebraic program written in FORM. Subsequent manipulation of integrands proceeds in a well-organized manner. The important point is that all higher-order integrals can be handled in the same manner, the necessary extension being straightforward. This is the reason why we are able to treat the algebra of higher-order cases with complete confidence.

APPENDIX B: NON-STATISTICAL ERROR IN NUMERICAL EVALUATION OF FEYNMAN INTEGRAL

Our integrand of Group IV is an algebraic function of more than 4000 terms, each term being a product of up to ten functions defined on a unit 10-dimensional cube:

$$0 \leq x_i \leq 1, i = 1, 2, \cdots, 10. \tag{B1}$$

FORTRAN codes of some integrals are as large as 100 kilobytes. These integrals are identical with the corresponding integrals for the electron vertices, the only difference being the value of the parameter m_e/m_μ. However, the behavior of muon integrals are strongly influenced by the presence of a singularity located at a distance of order $(m_e/m_\mu)^2$ just outside of the integration domain (B1), i.e., a unit cube. This makes numerical integration of some integrals more delicate or difficult compared with the electron case. This is the main (though not the only) source of the d-d problem in the muon $g - 2$ calculation.

Numerical integration of these integrals is carried out using an adaptive-iterative Monte-Carlo integration routine VEGAS [44]. It is the only effective method currently available to integrate such huge integrals. It is an adaptive-iterative integration routine based on random sampling of the integrand. In the ith iteration, the integral is evaluated by sampling it at points chosen randomly according to a distribution ρ_{i-1} (a step function defined by grids) constructed in the $(i - 1)$st iteration. This generates an approximate value I_i of the integral, its uncertainty σ_i, and the new distribution function ρ_i to be used in the next iteration. The distribution ρ_i is constructed in such a way that the grids concentrate in the region where the integrand is large. The construction of ρ_i in the $(i - 1)$st iteration involves a positive parameter β that controls the speed of "convergence" to a stable configuration. In most cases we chose $\beta = 0.5$. We may even be forced to choose $\beta = 0$ (no change in ρ), which is necessary in some difficult cases.

After several iterations I_i and σ_i are combined assuming that all iterations are statistically independent. The combined value and uncertainty are given by

$$I = \left[\sum_i (I_i/\sigma_i^2)\right] / \left[\sum_i (1/\sigma_i^2)\right], \quad \sigma = \left[\sum_i (1/\sigma_i^2)\right]^{-1/2}. \tag{B2}$$

For well-behaved integrals ρ_i converges rapidly to a (practically) stable configuration. Once ρ_i is stabilized, the error generated by VEGAS is (nearly) statistical and proportional to $\mathcal{N}^{-1/2}$, where $\mathcal{N}$ is the total number of data samplings.

After the point-by-point renormalization is made the integrand has the form

$$f = f_0 + \cdots + f_r, \tag{B3}$$

where f_0 is obtained directly from a Feynman diagram and $f_1, \ldots, f_r$ are terms needed to renormalize UV (and/or) IR divergences of f_0. Terms $f_0, \ldots, f_r$ are all divergent on the surface of the unit cube (B1). The sum f is mathematically well-defined and integrable.

This does not guarantee, however, that f is well-behaved on a computer. This is because expressions for $f_0, \ldots, f_r$ on computer are only as accurate as the number of digits in use (64 bits, 128 bits, etc.). In the part of the domain where $f_0, \ldots, f_r$ are singular, f loses most or all of significant digits and is affected severely by round-off errors. When this happens, I_i and σ_i become unreliable or even divergent. Note that this problem is an *inevitable* consequence of any computer calculation in which only a finite number of digits is available. We shall call it the digit-deficiency or d-d problem. In order to cope with the d-d problem before it upsets the integration, we have developed several strategies.

a. Stretching. The integrand f defined in (B3) may still have integrable singularities on some boundary surfaces, which can be removed by an appropriate change of variables. However, it is difficult to find analytically correct mapping because of the complicated structure of the integrand. A simple way to remove or weaken the d-d problem is the "stretching" defined as follows: Suppose VEGAS finds after several iterations that the integrand samplings tend to concentrate in the vicinity of an $(n - 1)$-dimensional surface, say $x_1 = 0$, perpendicular to the x_1 axis. Then the mapping

$$x_1' = x_1^{a_1}, \tag{B4}$$

where a_1 is a real number greater than 1, stretches out the domain near $x_1 = 0$ and random samplings in the x_1' variable give more attention to this region from the beginning of iteration. Also, the Jacobian $a_1 x^{a_1 - 1}$ of this mapping weakens the singularity. Similarly, the singularity at $x_1 = 1$ can be weakened by the stretching

$$x_1' = 1 - (1 - x_1)^{b_1}, b_1 > 1. \tag{B5}$$

Stretching is a one-to-one mapping of a unit hypercube onto itself. It may be applied to all variables independently. An appropriate stretching speeds up convergence of ρ considerably. Note also that different stretchings lead to statistically independent samplings of an integral which must give the same answer within error bars. This flexibility is important in assessing the reliability of results of integration. Of course, stretching does not always work well since it disregards the actual (and hard-to-identify) analytic structure of the integrand.

b. Splitting. Going from double precision (real*8) to quadruple precision (real*16) (or even higher) arithmetic is the most effective way to control the d-d problem. One practical obstacle is that real*16 slows down computation by a factor $20 \sim 30$. Thus we were not able to use real*16 extensively until massively parallel computers became readily available.

Actually, in many cases, real*16 is needed only in a small part of the integration domain. It is therefore useful to adopt the following strategy: Start the evaluation of a Feynman integral in real*8, which explores the integrand at high speed. If it identifies the region causing the *d-d* problem, split the integration domain into a small (rectangular) part in which the *d-d* problem occurs and the remainder. The difficult region is then evaluated in real*16, while the rest continues in real*8. This strategy has been very successful and most integrals have been evaluated in this manner.

Recently, a modified algorithm of VEGAS has been developed which makes this splitting local and automatic [42]. In this approach the integrand f is first evaluated at each point in real*8. The result is tested by computing the ratio

$$t = (f_+ + |f_-|)/|f_+ + f_-|, \tag{B6}$$

where $f_+(f_-)$ is the sum of positive(negative) terms of $f_0, \dots f_r$. If t is larger than an empirically selected number t_0, it signals a possible *d-d* problem. The integrand is then reevaluated in real*16 at the same spot. If the *d-d* problem is not severe, this method is very efficient and runs much faster than pure real*16. In difficult cases, however, a simple splitting may work faster since it does not require the overhead needed in computing (B6).

c. Freezing. Sometimes, it is very difficult to find a reasonable stretching that does not run into the *d-d* problem before it settles down to a (nearly) stable ρ. In such a case, one may freeze ρ by putting $\beta = 0$ few steps before the *d-d* problem becomes serious. The resulting ρ is not optimal so that it requires longer computing hours to achieve the desired statistical uncertainty.

d. Chopping. If procedures a, b, c fail to solve the *d-d* problem, one may restrict some integration axis (0, 1) to $(\delta, 1 - \delta)$, where $0 \leq \delta \ll 1$, to exclude the danger zone. This is referred to as *chopping*. The error introduced by *chopping* is of order $\delta^{1/2}(\ln\delta)^a$, where the positive number a can not be fixed without knowing the analytic structure. In practice it is sufficient to find a crude value of a by carrying out integration for several values of δ. When *chopping* is used, we must carry out full scale calculations for several δ (which require extra computing time). Note also that integration becomes more and more difficult as δ gets smaller. The difficulty in assessing the effect of chopping was the major source of nonstatistical uncertainty in earlier calculations.

Chopping can produce a crude approximate result vary rapidly. Thus it was used in early stage of our work to obtain estimates of a rough order of magnitude. However, it turned out to be not effective for obtaining more precise results. Thus it was abandoned entirely in the later phases of our work.

Our final results were obtained using *stretching*, *splitting*, and *freezing*, or their combinations. In most cases *stretching* and *splitting* are sufficient to solve the *d-d* problem. In some cases, however, even *splitting* was not sufficient. In the absence of higher precision arithmetic, the only effective way to control the *d-d* problem was *freezing*. In such a case it is still useful to divide the integration domain into several pieces and apply *freezing* in only one of them. Moreover, it is found to be useful to restrict the number of samplings per iteration to a relatively small number and use a very large number of iterations. This will enable us to accumulate large statistics while controlling the amount of wasted iterations to an acceptable level.

---

[1] G. W. Bennett *et al.*, Phys. Rev. Lett. **92**, 161802 (2004).

[2] G. W. Bennett *et al.*, Phys. Rev. Lett. **89**, 101804 (2002).

[3] H. N. Brown *et al.*, Phys. Rev. Lett. **86**, 2227 (2001).

[4] H. N. Brown *et al.*, Phys. Rev. D **62**, 091101 (2000).

[5] J. Bailey *et al.*, Phys. Lett. B **68**, 191 (1977); F. J. M. Farley and E. Picasso, in *Quantum Electrodynamics*, edited by T. Kinoshita (World Scientific, Singapore, 1990), p. 479.

[6] M. Davier, S. Eidelman, A. Höcker, and Z. Zhang, Eur. Phys. J. C **31**, 503 (2003).

[7] S. Ghozzi and F. Jegerlehner, Phys. Lett. B **583**, 222 (2004).

[8] K. Hagiwara, A. D. Martin, D. Nomura, and T. Teubner, Phys. Rev. D **69**, 093003 (2004).

[9] V. V. Ezhela, S. B. Lugovsky, and O. V. Zenin, hep-ph/0312114.

[10] A. Czarnecki and W. J. Marciano, Phys. Rev. D **64**, 013014 (2001).

[11] M. Davier and A. Höcker, Phys. Lett. B **435**, 427 (1998).

[12] S. Narison, Phys. Lett. B **513**, 53 (2001).

[13] J. F. de Troconiz and F. J. Yndurain, Phys. Rev. D **65**, 093001 (2002).

[14] M. Knecht and A. Nyffeler, Phys. Rev. D **65**, 073034 (2002); M. Knecht, A. Nyffeler, M. Perrottet, and E. de Rafael, Phys. Rev. Lett. **88**, 071802 (2002); M. Hayakawa and T. Kinoshita, hep-ph/0112102; J. Bijnens, E. Pallante, and J. Prades, Nucl. Phys. **B626**, 410 (2002); I. Blokland, A. Czarnecki, and K. Melnikov, Phys. Rev. Lett. **88**, 071803 (2002).

[15] M. J. Ramsey-Musolf and M. B. Wise, Phys. Rev. Lett. **89**, 041601 (2002).

[16] K. Melnikov and A. Vainshtein, hep-ph/0312226 [Phys. Rev. D (to be published)].

[17] KLOE Collaboration, A. Aloisio *et al.*, hep-ex/0407048.

[18] T. Blum, Phys. Rev. Lett. **91**, 052001 (2003).

[19] B. Krause, Phys. Lett. B **390**, 392 (1997).

[20] M. Knecht, S. Peris, M. Perrottet, and E. de Rafael, J. High Energy Phys. 11 (2002) 003.

[21] A. Czarnecki, W. J. Marciano, and A. Vainshtein, Phys. Rev. D **67**, 073006 (2003).

[22] V. W. Hughes and T. Kinoshita, Rev. Mod. Phys. **71**, S133 (1999).

[23] T. Kinoshita and M. Nio, Phys. Rev. Lett. **90**, 021803 (2003).

[24] T. Kinoshita and W. J. Marciano, in *Quantum Electrodynamics*, edited by T. Kinoshita (World Scientific, Singapore, 1990), p. 419.

[25] A. Wicht *et al.*, in *Proc. of 6th Symp. on Freq. Standards and metrology* (World Scientific, Singapore, 2002), p. 19.

[26] T. Kinoshita and M. Nio (to be published).

[27] S. G. Karshenboim, Yad. Fiz. **56**, 252 (1993) [Phys. At. Nucl. **56**, 857 (1993)].

[28] T. Kinoshita and M. Nio (to be published).

[29] P. J. Mohr and B. N. Taylor, Rev. Mod. Phys. **72**, 351 (2000).

[30] R. S. Van Dyck, Jr., P. B. Schwinberg and H. G. Dehmelt, Phys. Rev. Lett. **59**, 26 (1987).

[31] T. Kinoshita, Rep. Prog. Phys. **59**, 1459 (1996).

[32] T. Kinoshita, Nuovo Cimento B **51**, 140 (1967).

[33] S. Laporta, Nuovo Cimento Soc. Ital. Fis., B **106**, 675 (1993).

[34] S. Laporta and E. Remiddi, Phys. Lett. B **301**, 440 (1993).

[35] S. Czarnecki and O. Skrzypek, Phys. Lett. B **449**, 354 (1999).

[36] J. Aldins, S. Brodsky, A. Dufner, and T. Kinoshita, Phys. Rev. Lett. **23**, 441 (1969); Phys. Rev. D **1**, 2378 (1970).

[37] P. Cvitanovic and T. Kinoshita, Phys. Rev. D **10**, 4007 (1974).

[38] D. J. Broadhurst, A. L. Kataev, and O. V. Tarasov, Phys. Lett. B **298**, 445 (1993).

[39] T. Kinoshita, Phys. Rev. D **47**, 5013 (1993).

[40] T. Kinoshita and M. Nio, Phys. Rev. D **60**, 053008 (1999).

[41] T. Kinoshita, IEEE Trans. Instrum. Meas. **50**, 568 (2001).

[42] R. Sinkovits (to be published).

[43] S. Laporta, Phys. Lett. B **312**, 495 (1993).

[44] G. P. Lepage, J. Comput. Phys. **27**, 192 (1978).

[45] G. Källén and A. Sabry, Dan. Vidensk. Selsk. Mat.-Fys. Medd. **29**, 17 (1955).

[46] T. Kinoshita and W. B. Lindquist, Phys. Rev. D **27**, 867 (1983).

[47] A. H. Hoang *et al.*, Nucl. Phys. **B452**, 173 (1995).

[48] Note that $P(P4, P2)$ is simplified to $P4(P2)$.

[49] R. N. Faustov *et al.*., preprint TIFT-TH-90-8, revised version was published as Phys. Lett. B **254**, 241 (1991).

[50] H. Kawai, T. Kinoshita, and Y. Okamoto, Phys. Lett. B **260**, 193 (1991).

[51] J. Calmet and E. de Rafael, Phys. Lett. B **56**, 181 (1975).

[52] T. Kinoshita, H. Kawai, and Y. Okamoto, Phys. Lett. B **254**, 235 (1991).

[53] R. N. Faustov *et al.*, Phys. Lett. B **254**, 241 (1991).

[54] This spectral function was obtained by M. Nio.

[55] P. A. Baikov and D. J. Broadhurst, in *Proceedings of the 4th International Workshop on Software Engineering and Artificial Intelligence for High Energy and Nuclear Physics, Pisa, Italy, 1995* (AIHENP95, 1995), p.167

[56] T. Kinoshita, B. Nizic, and Y. Okamoto, Phys. Rev. D **41**, 593 (1990).

[57] T. Kinoshita, in *Quantum Electrodynamics*, edited by T. Kinoshita (World Scientific, Singapore, 1990), p. 218.

[58] T. Kinoshita and W. B. Lindquist, Phys. Rev. D **39**, 2407 (1989).

[59] B. E. Lautrup and M. A. Samuel, Phys. Lett. B **72**, 114 (1977).

[60] A. S. Elkhovsky, Yad. Fiz. **49**, 1059 (1989) [Sov. J. Nucl.Phys. **49**, 656 (1989)].

[61] J. A. M. Vermasseren, computer code FORM, ver. 2.3, 1998.

[62] An alternative is dimensional regularization. We do not consider it here since it is not known how to implement it in cases of high orders.

[63] R. Karplus and N. M. Kroll, Phys. Rev. **77**, 536 (1950).

[64] J. D. Bjorken and S. D. Drell, *Relativistic Quantum Fields* (McGraw-Hill, New York, 1965).

[65] N. Nakanishi, Prog. Theor. Phys. **17**, 401, (1957).